J. Fluid Mech. (2010), *vol.* 654, *pp.* 305–350.
doi:10.1017/S0022112010000625

Turbulent hydraulic jumps in a stratified shear flow

S. A. THORPE†

School of Ocean Sciences, Bangor University, Menai Bridge, Anglesey LL59 5AB, UK

(Received 12 August 2009; revised 27 January 2010; accepted 29 January 2010; first published online 14 May 2010)

The conditions are examined in which stationary hydraulic jumps may occur in a continuously stratified layer of fluid of finite thickness moving over a horizontal boundary at $z = 0$ and beneath a deep static layer of uniform density. The velocity and density in the flowing layer are modified by turbulent mixing in the transition region. Entrainment of fluid from the overlying static layer is possible. Results are expressed in terms of a Froude number, Fr, characterizing the flow upstream of a transition. A Froude number, Fr_*, is found that must be exceeded if conditions for the conservation of volume, mass and momentum fluxes across a hydraulic transition are satisfied. The condition $Fr > Fr_*$ is satisfied if the kinetic energy (KE) per unit area is greater than the potential energy per unit area, or if $\int_0^h [u^2(z) - z^2N^2(z)]\mathrm{d}z > 0$, in a flow of speed $u(z)$, in a layer of thickness h, with buoyancy frequency $N(z)$. In the particular case (referred to as an 'η profile') of a flow with velocity and density that are constant if $z \leqslant \eta h$, decrease linearly if $\eta h \leqslant z \leqslant h$, and in which $u(z) = 0$ and density is constant when $z \geqslant h$, long linear internal waves can propagate upstream, ahead of a stationary hydraulic jump, for Fr in a range $Fr_* < Fr < Fr_c$; here Fr_c is the largest Fr at which long waves, and wave energy, can propagate upstream in a flow with specified η. (Profiles other than the η profile exhibit similar properties.) It is concluded that whilst, in general, $Fr > Fr_*$ is a necessary condition for a hydraulic jump to occur, a more stringent condition may apply in cases where $Fr_* < Fr_c$, i.e. that $Fr > Fr_c$.

Physical constraints are imposed on the form of the flow downstream of the hydraulic jump or transition that relate, for example, to its static and dynamic stability and its stability against a further hydraulic jump. A further condition is imposed that relates the rate of dissipation of turbulent KE within a transition to the loss in energy flux of the flow in passing through the transition from the upstream side to the downstream. The constraints restrict solutions for the downstream flow to those in which the flux of energy carried downstream by internal waves is negligible and in which dissipation of energy occurs within the transition region.

Although the problem is formulated in general terms, particular examples are given for η profiles, specifically when $\eta = 0$ and 0.4. The jump amplitude, the entrainment rate, the loss of energy flux and the shape of the velocity and density profiles in the flow downstream of a transition are determined when $Fr > Fr_*$ (and extending to those with $Fr > Fr_c$) in a number of extreme conditions: when the loss of energy flux in transitions is maximized, when the entrainment is maximized, when the jump amplitude is least and when loss of energy flux is maximized subject to the entrainment into the transitions being made zero. The ratio of the layer thickness downstream and upstream of a transition, the jump amplitude, is typically at least 1.4 when

† Address for correspondence: 'Bodfryn', Glanrafon, Llangoed, Anglesey LL58 8PH, UK. Email: oss413@sos.bangor.ac.uk

jumps are just possible (i.e. when $Fr \sim Fr_c$). The amplitude, entrainment and non-dimensionalized loss in energy flux increase with Fr in each of the extreme conditions, and the maximum loss in energy flux is close to that when the entrainment is greatest. The magnitude of the advective and diffusive fluxes across isopycnal surfaces, i.e. the diapycnal fluxes characterizing turbulent mixing in the transition region, also increase with Fr. Results are compared to those in which the velocity and density profiles downstream of the transition are similar to those upstream, and comparisons are also made with equivalent two-layer profiles and with a cosine-shaped profile with continuous gradients of velocity and density. If Fr is larger than a certain value (about 7 and $> Fr_c$, if $\eta = 0.4$), no solutions for flows downstream of a transition are found if there is no entrainment, implying that fluid must be entrained if a transition is to occur in flows with large Fr. Although the extreme conditions of loss of energy flux, jump amplitude or entrainment provide limits that it must satisfy, in general no unique downstream flow is found for a given flow upstream of a jump.

1. Introduction: the problem posed

A spectacular hydraulic jump is sometimes observed in the atmosphere in the lee of the Sierra Nevada range. The phenomenon is illustrated in a photograph taken by Robert Simons reproduced in textbooks by Turner (1973) and Lighthill (1978). The transition is made visible by cloud and dust, and appears as a dramatic and abrupt increase, by a factor of about 5–10, in the thickness of the layer of air descending as an overflow of the mountain chain. The flow seems to be turbulent within and immediately behind the jump. Observations of turbulence and vertical diffusion in stratified flows over sills and through channels in the abyssal ocean, for example, in the Romanche Fracture Zone (Polzin *et al.* 1996; Ferron *et al.* 1998), the Atlantis II Fracture Zone through the SW Indian Ridge (Mackinnon, Johnston & Pinkel 2008) and the Lucky Strike segment of the Mid-Atlantic Ridge (St Laurent & Thurnherr 2007), has led to speculation that hydraulic jumps make a significant contribution to mixing in the deep ocean (Thurnherr *et al.* 2005; Thorpe 2007), but there are as yet no incontrovertible observations to prove the existence of these postulated flow transitions. In the relatively shallow water of Knight Inlet, British Columbia, however, Farmer & Armi (1999) have observed a stationary hydraulic jump in the lee of the sill where the downslope flow in a bottom layer during ebb tide increases in thickness from about 10 m to 50 m beneath an almost static, weakly stratified and relatively thick layer (see especially Farmer & Armi 1999, figures 7iid and 14). Hydraulic jumps may possibly also occur in cold water cascading downslope in the ocean and in lakes in winter (Thorpe & Ozen 2008, 2009), and there is some evidence (e.g. Stastna & Lamb 2008, figures 15*c* and 16) that jumps occurring in a stratified oceanic flow in the lee of submarine topography may lead to sediment suspension. Examples of stationary turbulent internal hydraulic jumps in the laboratory are provided by Wilkinson & Wood (1971) and Simpson (1997, see e.g. figures 12.4 and 12.14), and circular internal hydraulic jumps are described by Thorpe & Kavčič (2008).

It is therefore evident that stationary turbulent hydraulic jumps occur in at least some stratified shear flows. Here a theory is devised for jumps in stratified flows which follows that for a stationary hydraulic transition in a steady uniform inviscid constant density flow of depth h and speed u, e.g. in a hydraulic jump in a river downstream of a weir, where a Froude number, $Fr = u^2/c^2$, is defined as the square of the speed

of the flow divided by the maximum speed of waves relative to the flowing water or, more precisely, their maximum group velocity, which is equal to the speed of the longest waves, $c = \sqrt{gh}$. Application of conservation equations for volume, mass and momentum together with the condition that there is no increase in energy flux, proves sufficient to show that the Froude number of the flow approaching a stationary transition must exceed unity (i.e. the flow speed u is greater than the long-wave speed c) if a hydraulic jump is to be possible, and that the Froude number of the single-layer flow leaving the jump must then be less than unity and the water level must increase through the transition (Lighthill 1978). The change in water level in the jump can be related to the Froude number of the flow approaching the transition: the speed and depth of the flow downstream of a transition can be predicted in terms of their upstream values. Weak jumps, having a change in water depth less than about 0.3 times the water depth upstream of the jump (or $q = h_2/h_1 < 1.3$ and a Froude number <1.5), are generally undular in form, whereas transitions with highly turbulent fronts form when the jump amplitude is greater. A flux of energy is carried downstream within waves of an undular jump, whereas most of the loss in energy flux occurs through turbulent dissipation within jumps of greater amplitude. The critical Froude number of unity (when $u = c$) derived from the continuity equations also corresponds to that required to prevent waves – and wave energy – from propagating upstream from the stationary transition. It is shown later, however, that in a stratified flow, the conservation equations do not lead, in general, to a corresponding Froude parameter limit at which wave energy cannot propagate upstream. The implication is that stable hydraulic jumps in at least some stratified flows, with no upstream wave radiation possible, can occur only in conditions where the jump amplitude is substantial and where there is significant dissipation of energy in the transition region.

Much attention has been given to internal hydraulic jumps in two-layer flows, each layer uniform in density and velocity but with discontinuities at the interface, and in which the flow retains a two-layer structure after the transition. Yeh (1991), Baines (1995), Klemp, Rotunno & Skamarock (1997), Holland *et al.* (2002), Hassid, Regev & Poreh (2007) and Swaters (2009) provide examples and list further references. The flows that occur naturally in the ocean and atmosphere are, however, continuously stratified with no discontinuities in density or velocity. Examples of such flows are considered here. The situation in stratified shear flows is much more complex than in uniform single layers particularly when, as it appears in the transition in the lee of the Sierra Nevada, the flow becomes turbulent within the transition, and consequently its velocity and density structure is changed by mixing. In general, stratification allows internal waves to radiate vertically from the turbulent region in which a transition occurs, and flows may not be unidirectional. It consequently becomes difficult to compose physically realistic equations that express the conservation of flow properties from one side of the transition to the other. Stratification within a flowing layer, however, provides the advantage that, by comparing the density and velocity profiles on the two sides of a jump, it is possible to assess and quantify some aspects of mixing within the transition region, as explained in § 2.4 and shown in later figures (e.g. figure 8). (Nevertheless, it is hardly appropriate to suggest that this is one of the cases in which 'This can mean that the dynamics of a "simple" homogeneous fluid is actually more complicated than that of a stratified fluid' (Lighthill 1978, p. 451).)

We shall, for simplicity, confine attention to a particular case in which the flow approaching a stationary hydraulic jump from one side (the 'upstream' flow; 'upstream' and 'downstream' are used to indicate location relative to the transition) is unidirectional and in which the motion and variations in density of this flow are

confined to a layer of limited extent that lies above a horizontal boundary at $z=0$ and beneath a deep layer of zero velocity and uniform density, the latter precluding the possibility of upward internal wave radiation from the transition region. The fluid is supposed to be incompressible and viscosity is negligible except in its support of turbulent dissipation in the transition region. Free slip may occur at the lower boundary (although not necessarily) and, in deriving the equation of momentum conservation, the stress at the boundary is supposed to be negligible. It is assumed that the velocity and density structure of the upstream flow are specified and that the speed of this flow and its overall (or top to bottom) vertical variation in density can be represented by a non-dimensional number similar in form to a Froude number (to be denoted by Fr), but not necessarily or generally equal to a conventional Froude number, proportional to the flow speed divided by the group velocity of the fastest propagating waves.

Except in very limited conditions and unlike a transition in a single layer with uniform density and velocity, neither the structure of the density or the velocity of the flow leaving the transition (the 'downstream' flow) can be regarded as known. As mentioned above, turbulence and mixing within the transition region change the density profile (and may reduce its overall variation), and Reynolds stresses in the turbulent transition modify the velocity profile. The changes that occur are subject to conservation, stability and diapycnal flux conditions discussed in § 2. Attention is focussed on relatively large jumps that are consistent with those observed and in which, if akin to the jumps in single layers, turbulence rather than wave radiation may account for the loss in energy flux. (Simpson 1997, suggests that undular internal jumps occur if q is less than about 2, a value not substantiated by observations but somewhat greater than the limit of 1.3 for undular jumps in single layer hydraulics.)

A minimum value of the Froude number, Fr_*, at which the conservation equations at a hydraulic jump can be satisfied is found in § 3.

Several simple questions may be posed. For example, what is the minimum Froude number, Fr, of a given stratified upstream flow at which a hydraulic transition can occur? Is it equal to Fr_*? If Fr exceeds the minimum value for a jump, is the downstream flow similar to that which occurs upstream or when Fr is marginal? Is the downstream flow corresponding to a given upstream flow uniquely determined when a set of physically realistic conditions are applied? Do the jump amplitude and the loss of energy flux increase with Fr? How large is the diapycnal flux within the transition? Is entrainment of overlying fluid into a transition inevitable?

Such questions are addressed and investigated in detail for selected examples of the upstream flow defined in § 4.1. The speed of long small-amplitude internal waves can be calculated analytically in these cases (§ 4.2), as can the maximum Fr at which such waves can propagate in the upstream direction. This maximum Froude number is found in the examples to be generally greater than Fr_*, and is denoted as Fr_c, implying a critical value; it is a value of Fr that must be exceeded for stable jumps to be possible in the selected examples (§ 4.3). A value of Fr slightly greater than Fr_* is not always sufficiently large to prevent long small-amplitude internal waves from propagating upstream, and it follows that only jumps of finite amplitude can be stable. This implies a fundamental difference between hydraulic jumps in stratified flows and in single or two-layer flows that is additional to the other basic differences that exist between these continuously stratified and two-layer shear flows (e.g. those differences identified by Thorpe & Kavčič 2008).

Downstream flows that have similar density and velocity profiles to those upstream are considered in § 5 but are restrictive and, as is shown later (e.g. figures 7 and 10),

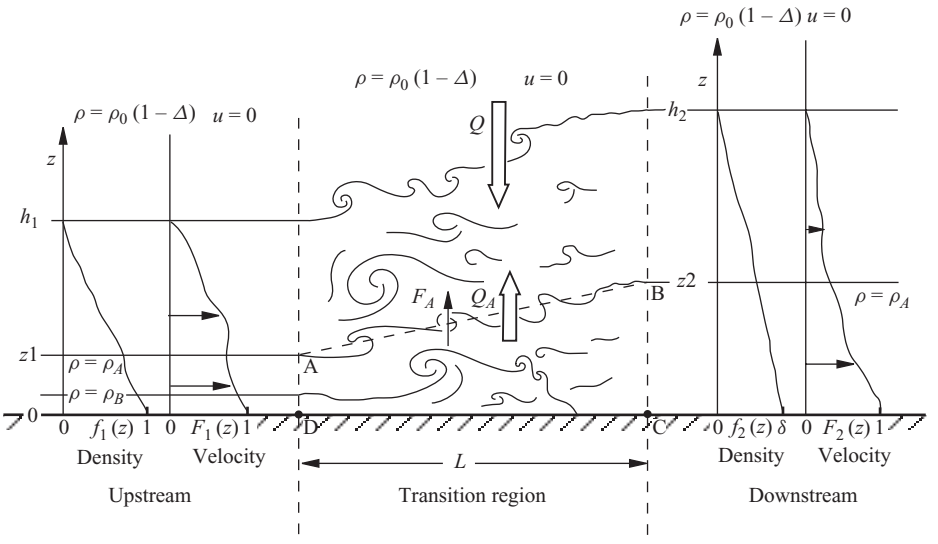

FIGURE 1. A hydraulic jump or transition in stratified shear flow. Profiles of density ($f_i(z)$) and velocity ($F_i(z)$) ($i = 1$, upstream and $i = 2$, downstream) in the layer are sketched in the flowing layer beneath the deep stationary layer of uniform density $\rho_0(1 - \Delta)$. Q is the flux of volume entering the flowing region within the transition. An isopycnal, density $\rho = \rho_A$, is shown, entering the transition at level $z = z1$ and leaving it at level $z2$, as discussed in § 2.4. The line AB denotes the notional mean location of the isopycnal surface within the turbulent transition region. AD is a surface across which the upstream flow below the selected isopycnal enters the transition, and CD the region of the downstream flow below the isopycnal after turbulence generated within the transition has decayed. The quantities Q_A and F_A represent the upward advective volume flux and of the diffusive flux of mass across the isopycnal within the transition. (There is no flux through the horizontal plane, $z = 0$.) As a result of mixing, the maximum density of the upstream flow, $\rho_0(1 + \Delta)$ at $z = 0$, may exceed the maximum density of the downstream flow, $\rho_0[1 + \Delta(2\delta - 1)]$ at $z = 0$, so $\delta < 1$. There are then (as sketched) upstream ρ_B isopycnals that intersect the $z = 0$ boundary and do not re-emerge in the flow downstream of the transition region.

not necessarily representative. A general expression for the form of the downstream flow is proposed in § 6.1. The main results of the analysis of transitions when $Fr > Fr_*$ and covering a range of Fr extending beyond Fr_c are described in §§ 6.2–6.4 and are illustrated in figures. These include profiles of the possible downstream flows that can occur under the set of conditions specified in § 2 and in four extreme cases defined in § 6.1, in addition to the diapycnal fluxes within the transition region necessary for the downstream flows to be possible. The results and applications are summarized, extended and discussed in § 7 to which readers wishing to avoid all the details, but to see the main conclusions, are referred. Details of the analysis and methodology outlined in the main text are given in eight appendices.

2. Conservation and conditions on the upstream and downstream flows

2.1. *The upstream and downstream flows*

Following Thorpe & Ozen (2007), we shall assume that the velocity upstream and downstream of the transition is uniform in a horizontal direction and depends only on the vertical coordinate, z, as sketched in figure 1. The velocity is given by

$$u_i(z) = U_i F_i(z/h_i) \quad \text{when } 0 \leqslant z \leqslant h_i, \tag{1}$$

where subscript $i=1$ indicates the steady upstream flow approaching a jump and $i=2$ indicates the steady downstream flow beyond the jump, with $F_i(0)=1$. The velocity $u_i(z)=0$ when $z>h_i$. The density is

$$\rho_i(z)=\rho_0[1-\Delta+2\Delta f_i(z/h_i)] \text{ when } 0\leqslant z\leqslant h_i, \tag{2}$$

with $\rho_i(z)=\rho_0(1-\Delta)$ when $z>h_i$, Both F_i and f_i are positive functions of $z/h_i(=x)$ which define the velocity and density 'profiles' (i.e. variation with z.). The reference density ρ_0, the measure of density variation Δ and the velocity measures U_i are all positive. These conditions imply that the velocity both ahead and beyond the transition is positive, i.e. in a direction from upstream to downstream, at all levels $z<h_i$, with no reversed flow, consistent with the assumption of a unidirectional flow and with no source of fluid at any level, z, beyond the transition. The density in $z>h_i$ is taken to be uniform so that no energy can be lost through the upward radiation of internal waves from the transition. We shall insist that $F_i(1)=0$ and $f_i(1)=0$ making the velocities and densities in the upstream and downstream flows continuous at $z=h_i$. The functions, $\mathrm{d}f_i(z/h_i)/\mathrm{d}z$, are taken to be $\leqslant 0$ to ensure static stability, and $f_1(0)=1$, so defining the maximum upstream density as $\rho_0(1+\Delta)$ and $2\rho_0\Delta$ as the density change from $z=0$ to $z=h_1$. Further, we define a parameter, $\delta\leqslant 1$, so that the maximum density in the downstream flow (found at $z=0$, since $\mathrm{d}f_i(z/h_i)/\mathrm{d}z\leqslant 0$) is given by (2) with $f_2(0)=\delta$: $\rho_2(0)=\rho_0[1-\Delta+2\Delta\delta]$). This must be less than or equal to the maximum density upstream (there being no mechanism within the transition to increase the density). For convenience, we let $f_2(x)=\delta f_2'(x)$, so that the new density function $f_2'(x)$ decreases monotonically from 1 at $x=0$ to 0 at $x=1$.

2.2. *Entrainment and the conservation of fluxes*

Conservation laws relating to the fluxes of volume, mass and momentum are satisfied across the transition region. For convenience, the conservation equations given by Thorpe & Ozen (2007, with an amendment: Thorpe & Ozen 2009) are reproduced in the Appendix A (see (A 1)–(A 6)). The turbulence within the transition region may entrain fluid from above the moving upstream layer at a rate, Q, and this entrained fluid contributes to the downstream fluxes (figure 1). A parameter P is used to provide a non-dimensional representation of the entrained flow:

$$P=1+Q\Big/\left(U_1h_1\int_0^1 F_1(x)\,\mathrm{d}x\right). \tag{3}$$

The entrainment parameter P is equal to the downstream volume flux divided by the upstream volume flux, and $(P-1)$ is equal to the volume flux of fluid Q, entrained in the transition divided by the upstream volume flux. There is no entrainment when $P=1$. Using (A 5), P may be written as

$$P=P_0/\delta, \tag{4}$$

where

$$P_0=\int_0^1 f_1(x)F_1(x)\,\mathrm{d}x\int_0^1 F_2(x)\,\mathrm{d}x\Big/\left(\int_0^1 f_2'(x)F_2(x)\,\mathrm{d}x\int_0^1 F_1(x)\,\mathrm{d}x\right) \tag{5}$$

depends on specified profiles, F_1 and f_1 of the upstream flow, and on F_2 and f_2', the functions that define the (generally unknown) shape of the downstream flow.

There are two important limits implied by (4). If there is no entrainment, $P=1$, and so $\delta=P_0$, which must be $\leqslant 1$. Alternatively, if there is no mixing within the flow so that its maximum density is not reduced as it passes through the transition, then

$\delta = 1$, and so $P = P_0$, $\geqslant 1$ since fluid is assumed to be entrained, and not detrained, within the transition.

A number that characterizes the upstream flow and has the form of a Froude number is

$$Fr = U_1^2/(g\Delta h_1), \tag{6}$$

and when the flux of momentum is conserved, (A 6) relates Fr to the amplitude of the change in levels, $q = h_2/h_1$, and to integral properties of the upstream and downstream flows. (A Froude number might also be characterized by $Fr = U_1^2/(2g\Delta h_*)$, where h_* is the mean depth of the bottom layer and 2Δ is the density change across the moving layer. Neither form is necessarily equal to the ratio of the flow speed to the propagation speed of long internal waves and so, in general, neither is equal to a conventionally defined Froude number.) Using (4), (A 6) can be written as

$$Fr = 2q\left[q^2P_0\int_0^1 xf_2'(x)\,\mathrm{d}x - P\int_0^1 xf_1(x)\,\mathrm{d}x\right]\Big/\left[P\int_0^1 F_1^2(x)\,\mathrm{d}x\left\{q - P^2\right.\right.$$
$$\left.\left.\times\int_0^1 F_2^2(x)\,\mathrm{d}x\left(\int_0^1 F_1(x)\,\mathrm{d}x\right)^2\Big/\left[\int_0^1 F_1^2(x)\,\mathrm{d}x\left(\int_0^1 F_2(x)\,\mathrm{d}x\right)^2\right]\right\}\right], \tag{7}$$

which must be positive.

Another condition must be satisfied: the loss of the energy flux in the flow as it passes through the transition from the upstream to the downstream cannot be negative since energy is not created within the transition; energy can only be maintained, lost in turbulent dissipation or radiated by internal waves that carry energy downstream. From (A 7) the change of the energy flux per unit width in the transition, E', is expressed in non-dimensional form as

$$E \equiv E'\left(\rho_0 g\Delta h_1^2 U_1\right) = \left\{(Fr/2)\left[\int_0^1 F_1^3\,\mathrm{d}x - \int_0^1 F_2^3\,\mathrm{d}x\left(\int_0^1 F_1\,\mathrm{d}x\Big/\int_0^1 F_2\,\mathrm{d}x\right)^3 P^3/q^2\right]\right\}$$
$$+2\left[\int_0^1 xf_1F_1\,\mathrm{d}x + \int_0^1 F_1\int_x^1 f_1(y)\,\mathrm{d}y\,\mathrm{d}x\right] - 2q\left[\int_0^1 f_1F_1\,\mathrm{d}x\Big/\int_0^1 f_2'/F_2\,\mathrm{d}x\right]$$
$$\times\left[\int_0^1 xf_2'/F_2\,\mathrm{d}x + \int_0^1 F_2\int_x^1 f_2'/(y)\,\mathrm{d}y\,\mathrm{d}x\right]. \tag{8}$$

The first term on the right-hand side, that in the $\{\ldots\}$ brackets, is proportional to the rate of loss of kinetic energy (KE) flux in the transition. The remainder is the sum of the work done by the pressure and the rate of loss of potential energy flux.

The constraints imposed so far are

(a) the upstream and downstream flows are unidirectional;

(b) the density is uniform and the flow at rest when $z \geqslant h_i$, $i = 1, 2$; no waves can be radiated upwards from a transition;

(c) the upstream and downstream flows are stably stratified (with $\mathrm{d}f_i(z/h_i)/\mathrm{d}z \leqslant 0$);

(d) the maximum density of the downstream flow is not greater than that upstream, so $\delta \leqslant 1$;

(e) fluid is not detrained in the transition; there is positive or no entrainment, so $P \geqslant 1$;

(f) the change in energy flux in the transition cannot be negative: $E \geqslant 0$; and

(g) values of q, P, $f_2'(x)$ and $F_2(x)$ cannot be such that Fr, given by (7), is negative.

2.3. *Stability*

Additional conditions are imposed on the downstream flow to ensure that it is stable:

(h) the downstream flow is dynamically stable. To ensure this we confine the possible downstream flows to those with a minimum gradient Richardson number, Ri_2, that is sufficiently large to ensure dynamical stability (e.g. $\min(Ri_2) \geqslant 1/4$), noting that condition (c) in the downstream flow becomes redundant if $\min(Ri_2) \geqslant 0$. (The condition $\min(Ri_2) \geqslant 1/4$, selected for simplicity, 'ensures' stability – it is sufficient but not necessary: the flow may be stable to small disturbances when $\min(Ri_2) < 1/4$ (see e.g. Thorpe & Ozen 2007; Thorpe & Liu 2009). Although we shall examine only cases where the upstream flow is stably stratified, we shall not insist it is dynamically stable, because in reality this may not be the case, e.g. where it is composed of Antarctic Bottom Water accelerating through a slowly narrowing passage through the Mid-Atlantic Ridge or after the acceleration of a downslope flow before the dynamical instability has resulted in the growth of Kelvin–Helmholtz billows.); and

(i) the downstream flow is not able to undergo a further transition; it is 'stable' to further transition. This is expressed by the condition $S \leqslant 1$ ((A 10), although this may be too severe a constraint: see Appendix A).

Using (1), (2) and (A 4), $\min(Ri_2)$ can be expressed as

$$\min(Ri_2) = (q/P)^3 \left[(2P_0^3/Fr) \left(\int_0^1 f_2' F_2 \,\mathrm{d}x \Big/ \int_0^1 f_1 F_1 \,\mathrm{d}x \right)^2 \right] \times \min[-\mathrm{d}f_2'/\mathrm{d}x)/(\mathrm{d}F_2/\mathrm{d}x)^2]. \quad (9)$$

With (4), and since $f_2(0) = \delta$, (A 10) gives

$$S = Fr\,P^4 \Big/ \left\{ 4q^3 \left[\int_0^1 x f_2' \,\mathrm{d}x \Big/ \int_0^1 F_2^2 \,\mathrm{d}x \right] \left[\int_0^1 f_2' F_2 \,\mathrm{d}x \Big/ \int_0^1 f_1 F_1 \,\mathrm{d}x \right]^2 P_0^4 \right\}. \quad (10)$$

2.4. *Diapycnal fluxes within the transition*

Conditions (a)–(i) prove generally insufficient to constrain solutions for the downstream flow to a single form.

The relation of mixing within the transition to the change in energy flux is now investigated. We introduce a condition that relates the total rate of loss of energy flux, E', the difference between fluxes of energy in the upstream and downstream flow, to the flux of volume and mass (i.e. the diapycnal fluxes) across isopycnal surfaces. An isopycnal surface with density ρ_A is selected, one that appears in the upstream flow at levels $z1$ and in the downstream flow at levels $z2$, as shown in figure 1. We examine the fluxes into the region ABCD spanning the transition, where AB is the notional mean location of the ρ_A isopycnal within the region of turbulent mixing in the transition, and CD lies on the horizontal plane at $z = 0$. (If, because of mixing within the transition, $\delta < 1$, the full range of density in the upstream flow will not be found in the downstream flow; some upstream isopycnals, those with density greater than $\rho_0(1 - \Delta + 2\delta\Delta)$, will 'disappear' through mixing within the transition region, as does the $\rho = \rho_B$ isopycnal in figure 1. In this case there is no flux in the downstream flow below any isopycnal that disappears within the transition – there is no corresponding isopycnal downstream – and the upstream fluxes of volume and mass below the isopycnal are then equal to the upward vertical fluxes through the isopycnal within the transition region. An example is discussed in § 6.2 in connection with figures 7(d) and 8(b).)

There are both advective and diffusive fluxes across the isopycnal surface AB. Let Q_A be the net upward flux of volume across AB (i.e. the advective flux), and F_A be the net upward diffusive flux of density. Equations for the fluxes are derived in Appendix B and used to express Q_A and F_A in non-dimensional forms:

$$Q_* \equiv Q_A \Big/ \left(U_1 h_1 \int_0^1 F_1 \, \mathrm{d}x \right) \text{ and } F \equiv F_A / \Delta\rho_0 U_1 h_1, \tag{11}$$

given by (B 3) and (B 7), respectively, with terms that are known once the upstream flow is specified and a particular downstream flow is selected or determined.

The eddy diffusion coefficient K_v in the stratified turbulent region of the transition can be expressed as

$$K_v = \Gamma \varepsilon / N^2, \tag{12}$$

where Γ is a mixing efficiency factor, usually taken to be about 0.2 (an approximate upper limit; Osborn 1980), ε is the rate of dissipation of turbulent KE per unit mass and N is the mean buoyancy frequency given by

$$N^2 = -(g/\rho_0)\, \mathrm{d}\rho/\mathrm{d}z, \tag{13}$$

where ρ is the mean density at level z.

The upward diffusive flux per unit width across the isopycnal surface within the transition is

$$F_A = -L K_v \, \mathrm{d}\rho/\mathrm{d}z, \tag{14}$$

where L is the length of the transition region and, since $\mathrm{d}\rho/\mathrm{d}z \leqslant 0$, F_A must be $\geqslant 0$ to ensure that K_v is positive. Eliminating N and $K_v \mathrm{d}\rho/\mathrm{d}z$ from (12)–(14):

$$\varepsilon = g F_A / \Gamma L \rho_0, \tag{15}$$

and the mean rate of loss of turbulent KE in the transition region is therefore

$$\langle \varepsilon \rangle \rho_0 L (h_1 + h_2)/2 = (g \langle F_A \rangle / 2\Gamma) h_1 (1 + q), \tag{16}$$

where '$\langle\ \rangle$' denotes vertically average values and $q = h_2/h_1$. (The depth of the transition has been approximated as $(h_1 + h_2)/2$. The possible percentage error is $100(q-1)/(q+1)$, or 50 % if $q = 3$.) The mean rate of turbulent dissipation is equal to the loss of energy flux per unit width in the transition E' given by (8), if

$$\Gamma = \langle F \rangle (1 + q)/2E, \tag{17}$$

where it is assumed that all the loss in energy flux occurs within the transition region, none by downstream internal wave radiation in an undular jump.

This provides two further constraints:

(j) the density flux F_A within the transition must be positive upwards (and so positive downgradient, consistent with a positive K_v in (14)), and

(k) the loss of energy flux in the transition, E, must be consistent with the mean diapycnal flux, $\langle F \rangle$, within the transition region, giving a value of Γ estimated from (17) of about 0.2.

2.5. *Extreme values of q, P and E*

Although these added constraints eliminate some solutions for the downstream flow that, otherwise, appear plausible, the downstream flow is not necessarily found to be uniquely determined (i.e. for some selected upstream flows, there is more than one choice of the downstream flow that satisfies all the conditions). We shall therefore also resort to finding downstream flow solutions for specified upstream flows that

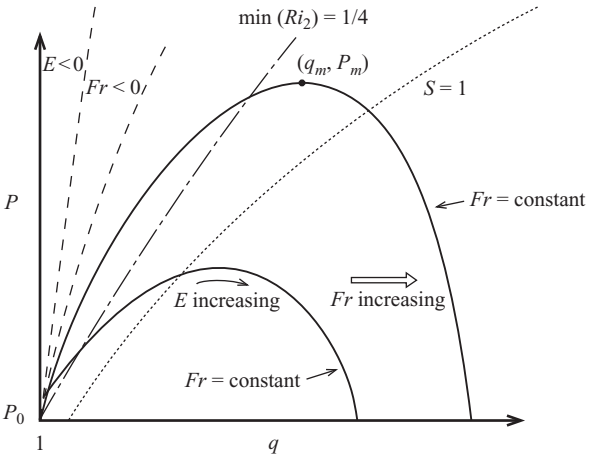

FIGURE 2. Sketch showing two lines of constant (but different) $Fr > 0$ in the (q–P) plane for given upstream and selected downstream flows. $Fr < 0$ between the dashed lines. $E < 0$ near the P axis, and $E \geqslant 0$ and increases to the right where $Fr > 0$. The point where the entrainment coefficient P is greatest on a curve of constant Fr (see (18) and (19)) is marked by the point (q_m, P_m). The curves $\min(Ri_2) = 1/4$ and $S = 1$ which specify boundaries of the regions in which conditions (h) and (i) are satisfied are shown. 'Stable' conditions are found to the right of these curves. The relative positions of the curves and the point (q_m, P_m) depend on the chosen upstream and downstream flows. (The curve $S = 1$ lies to the right of the point (q_m, P_m) and the line $\min(Ri_2) = 1/4$, both here and in the corresponding curves shown in figure 5. In such cases the largest value of P for which conditions (h) and (i) are satisfied is where $S = 1$ intersects Fr = constant. More commonly, however, it appears that the curve $\min(Ri_2) = 1/4$ – and condition (h) – determines the limiting condition.)

occur at extreme values of q, P or E expressed explicitly as cases (i)–(iv) in § 6.1. A condition that the transition involves the greatest loss of energy flux, E, provides information about the bounds on the possible dissipation from a given flow within a hydraulic transition, and the values of P and q at which these bounds are reached are discussed in Appendix C in the limited conditions of fixed F_2 and f_2'.

The general form of the relationship between q and P for a particular choice of the downstream flow is sketched in figure 2. (Specific examples when the upstream and downstream flows have 'similar' properties are shown later in figure 5.) The ranges of q and P which satisfy (7) (i.e. the ranges of those points (q, P) that are on a curve Fr = constant for a given upstream flow) are limited, and they will vary with the form of the downstream flow. The range of physically realistic values is also limited by the condition (f): $E \geqslant 0$, and condition (g): $Fr > 0$; only for sufficiently large q are the conditions satisfied. The relative locations of the curves $\min(Ri_2) = 1/4$ and $S = 1$ which specify boundaries of the regions in which conditions (h) and (i) are satisfied (those at relatively large values of q), all vary with the downstream flow given by F_2 and f_2', on which the value P_0 also depends.

Equation (7) provides a relation between q and P for given Fr, F_1, f_1, F_2 and f_2'. Differentiating with respect to q it is found that there is a single value q_m at which P is a maximum given by

$$q_m = (1/\gamma)\left\{\left[\gamma\left(Fr\int F_1^2\,\mathrm{d}x + 2\int x f_1\,\mathrm{d}x\right) - 2P_0\int x f_2'\,\mathrm{d}x\right]\Big/\left(\chi\, Fr\int F_1^2\,\mathrm{d}x\right)\right\}^{1/3}, \tag{18}$$

when

$$P \equiv P_m = \gamma q_m^2, \tag{19}$$

where

$$\gamma = 6P_0 \int x f_2' \,\mathrm{d}x \Big/ \left(Fr \int F_1^2 \,\mathrm{d}x + 2 \int x f_1 \,\mathrm{d}x \right) \tag{20}$$

and

$$\chi = \int F_2^2 \,\mathrm{d}x \left(\int F_1 \,\mathrm{d}x \right)^2 \Big/ \left[\int F_1^2 \,\mathrm{d}x \left(\int F_2 \,\mathrm{d}x \right)^2 \right], \tag{21}$$

all integrals being from $x = 0$ to $x = 1$. Substitution of the values, q_m and P_m into (8) enables the rate of energy loss to be found when the entrainment rate is greatest. The downstream flow at q_m and P_m may not, however, satisfy all the conditions (f), (h) and (i) required to ensure that it is physically possible; the point (q_m, P_m) in figure 2 may lie to the left of any one of the curves $E = 0$, $\min(Ri_2) = 1/4$ and $S = 1$.

In § 4 we shall select specific profiles of upstream velocity and density to provide illustrative examples, and in subsequent sections examine the possible downstream profiles that comply with the constraints and which emerge after transition from these particular upstream profiles.

3. A Froude number necessary for a transition

Following the theory of single-layer flows (§ 1), we define the Froude number Fr_* to be that of the smallest upstream flow U_1 at fixed h_1 and Δ, for which the conservation equations can be satisfied, supposing (as in the theory of hydraulic jumps in single and two-layer flows) that the flow profiles are unchanged so that $F_2 = F_1$ and $f_2' = f_1$, so that from (5) $P_0 = 1$. As shown in Appendix D, the limiting value of Fr occurs in the limit when there is no entrainment ($P = 1$), and when the downstream flow depth is identical to that upstream ($q = 1$). In this limit, (7) gives

$$Fr_* = 4 \int_0^1 x f_1(x) \,\mathrm{d}x \Big/ \int_0^1 F_1^2(x) \,\mathrm{d}x, \tag{22}$$

and (8) implies that the loss of energy flux E is zero. The value, $Fr_* = 2$, found for a two-layer flow by putting $F_1 = f_1 = 1$, is in accordance with the critical Froude number required for a jump in the two-layer flows.

Equation (22) can be interpreted in more physical terms: $Fr = Fr_*$ when

$$U_1^2/(g\Delta h_1) = 4 \int_0^1 x f_1(x) \,\mathrm{d}x \Big/ \int_0^1 F_1^2(x) \,\mathrm{d}x, \tag{23}$$

or cross-multiplying and using (1) and (2), when

$$\int_0^H [\rho_0 u_1^2(z)/2] \,\mathrm{d}z = g \int_0^H [\rho_1(z) - \rho_1(H)] \, z \,\mathrm{d}z, \tag{24}$$

with $H = h_1$ and where $u_1(z)$ is the upstream velocity. The Froude number exceeds Fr_* when

$$\int_0^H [\rho_0 u_1^2(z)/2] \,\mathrm{d}z > g \int_0^H [\rho_1(z) - \rho_1(H)] \, z \,\mathrm{d}z, \tag{25}$$

or when the KE is greater than the relative potential energy, both energies being calculated per unit horizontal area. Integrating by parts, (25) can also be written as

$$\int_0^H \left[u_1^2(z) - z^2 N_1^2(z)\right] \mathrm{d}z > 0, \tag{26}$$

where $N_1(z)$ is the buoyancy frequency.

It is necessary that the Froude number Fr_* must be exceeded if a transition is to occur. It is not, however, always the smallest Fr required for a stable jump, as shown in the next section.

4. Selected examples of the upstream flow and wave propagation

4.1. *The two examples*

To demonstrate the application of the analysis, and to provide some representative results, we choose as specific examples two upstream flows represented by F_1 and f_1, respectively, that are continuous and, for simplicity, with velocity and density profiles that are identical.

The 'η profile' is defined as

$$F_1(x) = f_1(x) = \begin{cases} 1, & \text{if } 0 \leqslant x \leqslant \eta \leqslant 1, \\ (1-x)/(1-\eta), & \text{if } \eta \leqslant x \leqslant 1, \end{cases} \tag{27}$$

where $x = z/h_1$. This has discontinuous gradients at $x = \eta$ and $x = 1$, and provides examples of flow ranging from a uniform gradient extending to $z = 0$ when $\eta = 0$, to a two-layer structure when $\eta = 1$. Profiles for $\eta = 0$ and $\eta = 0.4$ are shown in figure 3(*a*, *b*), respectively, these being values of η selected for later study.

The minimum Richardson number of the η profile is

$$\min(Ri_1) = 2(1-\eta)/Fr. \tag{28}$$

Although large for relatively small values of Fr, $\min(Ri_1)$ is equal to 1/4 when $Fr = 8(1-\eta)$, indicating possible instability in the upstream flow at greater values of Fr. (The flow given by (27) with $\eta = 0$ is however found to be stable to small disturbances for all $Ri \geqslant 0$.) The limiting Froude number Fr_* (see (22)) is given by

$$Fr_* = 2(1 + \eta + \eta^2)/(1 + 2\eta), \tag{29}$$

as shown in figure 4; $Fr_* = 2.0$, 1.73 and 2.0 when $\eta = 0$, 0.4, and 1.0, respectively (the latter being the two-layer flow). From (28), $\min(Ri_1) = 2(1-\eta)/Fr_*$, or 1.0 and 0.692 when $\eta = 0$ and 0.4, respectively. (When $\eta < 0.7676$, $\min(Ri_1) > 1/4$ so the downstream flow at $P = q = 1$ is then dynamically stable, in accord with condition (*h*).)

The second example, devised to remove the discontinuous gradients of the η profile, is the 'cosine profile' defined as

$$F_1(x) = f_1(x) = \begin{cases} 1, & \text{if } 0 \leqslant x \leqslant l/h_1' < 1, \\ \{1 + \cos[\alpha\pi(x - l/h_1')]\}/2, & \text{if } l/h_1' \leqslant x \leqslant 1, \end{cases} \tag{30}$$

where $x = z/h_1'$ and $\alpha(1 - l/h_1') = 1$. The derivatives of $F_1(x)$ and $f_1(x)$ are continuous.

For later comparison of results derived for the two profiles and the effects of the discontinuous gradients in the η profile, h_1' and l are chosen so that the slopes of F_1

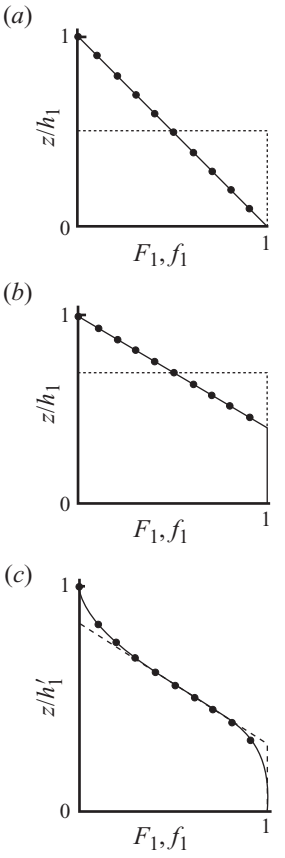

FIGURE 3. The matched η and corresponding two-layer profiles (dotted) with (*a*) $\eta = 0$ and (*b*) $\eta = 0.4$. (*c*) The cosine profile corresponding to $\eta = 0.4$, which is given by the dashed line. The large dots show density values specifying isopycnal surfaces, $f_1 = (1 - 0.1n)$, from $n = 1$ (the lowest) to $n = 10$ (at $z = h_1$), across which the volume and mass fluxes are calculated within the transition in §§ 6.2–6.4.

and f_1 in the two cases are equal at the level $z = h_1(1 + \eta)/2$, the mid-height of the uniform gradient in (27). This is so if

$$h_1' = h_1[2(1+\eta)+\pi(1-\eta)]/4,\ \alpha = 2/[\pi(1-\eta)] \text{ and } l = h_1[2(1+\eta)-\pi(1-\eta)]/4. \quad (31)$$

(The height of the uniform layer, l, is zero if $\eta < 0.222$, in which case $f_1(0) = F_1(0) \neq 1$. Such cases are excluded from later discussion by selecting $\eta = 0.4$.) The vertically integrated fluxes of both volume and mass in the η and equivalent cosine profiles are then equal. The form of the cosine profile matched to an η profile with $\eta = 0.4$ is shown in figure 3(*c*). The minimum Richardson number of the cosine profile is

$$\min(Ri_1) = 8(1 - \eta)/\{Fr[2(1 + \eta) + \pi(1 - \eta)]\}, \quad (32)$$

where Fr is the Froude number, $U_1^2/g\Delta h_1'$. The corresponding Froude number of the cosine profile, $Fr_* = U_1^2/g\Delta h_1'$, is

$$Fr_* = 2[4(1 + \eta)^2 + (\pi^2 - 8)(1 - \eta)^2]/[8 - \pi + (8 + \pi)\eta], \quad (33)$$

so that $Fr_* = 1.56$ when $\eta = 0.4$. (The Froude number of the equivalent η profile, $U_1^2/g\Delta h_1$, is 1.83. From (27), $\min(Ri_1)$ of the cosine profile when $Fr = Fr_*$ is 0.657 when $\eta = 0.4$.)

Possible forms of the downstream flows are examined in the following sections, taking their profiles to be similar to the upstream flows (in § 5) or having general forms composed of a linear variation in z plus a series of sinusoidal terms (in § 6). We shall compare results found for the continuously stratified flows with those for matched two-layer flows that have bottom layers uniform in velocity and density and of thickness $h_1(1+\eta)/2$ as shown in figure 3. For the selected upstream flows, this allows assessment of the effect of representing a transition in a continuously stratified flow by its two-layer equivalent. [At first sight it may appear that when, as chosen here, the speed of the transition in the two-layer flow (the solution with $\eta = 1$) matches that of the overlying layer (both being zero), we have a particular example of the situation described by Thorpe (1974) and by Saffman & Yuen (1982) in which (with the replacement of g by the reduced gravity, $2\Delta g$) the solution is 'exactly the same' as that of a single layer (even accounting for finite-amplitude effects!). The equivalence depends, however, on there being hydrostatic pressure in the upper layer (which is satisfied) and on Bernoulli's equation holding in the lower layer (which is not satisfied in a turbulent transition). In the given restricted conditions of zero speeds of both the overlying flow and the jump, the shape of the interface in a two-layer jump will indeed be identical to the free-surface shape of a hydraulic jump in a single layer, but only in cases when jumps are weak with no generation of turbulence.]

4.2. *Wave propagation in an η profile*

The speed of long internal waves in flows of the form (27) can be found analytically as outlined in Appendix E. When $\eta < 2/3$, there are upstream travelling waves if $Fr = U_1^2/g\Delta h_1 < 8(1-\eta), = Fr_c$, say, i.e. when $\min(Ri_1) > 1/4$; e.g. when $Fr < 8.0$ and 4.8 if $\eta = 0$ and 0.4, respectively. The curve $Fr = Fr_c$ gives the maximum value of Fr at which waves can propagate upstream; at values of $Fr > Fr_c$ there are no upstream travelling waves. The curve $Fr = Fr_c$ for $0 \leqslant \eta \leqslant 1$ is shown in figure 4, together with some contours of $(-c/U_1)$, the speeds of the fastest (mode 1) upstream travelling waves normalized with the flow speed U_1.

4.3. *A minimum Fr for a stable jump in an η profile*

Except when $\eta = 1$, the values of Fr_* are less than Fr_c (figure 4); they are in the range of Fr in which upstream travelling internal waves can occur. Long upstream travelling waves or columnar modes (McEwan & Baines 1974; Baines 1995) exist at Froude numbers in the range $Fr_* < Fr < Fr_c$, transferring energy upstream from a stationary jump and modifying the upstream flow. As explained in Appendix E, the long waves have properties that are in accord with those leading to a convergence of characteristics and the formation of hydraulic jumps in single layers (e.g. Lighthill 1978). However (unlike the free-surface hydraulic jumps described in § 1 or jumps in two-layer flows) when $\eta < 1$ the value of Fr_* derived from the continuity equations differs from that required for no upstream wave propagation; stratified flows support an infinite set of wave modes, and a hydraulic jump corresponds to a transition where the modes, in combination, lead to a change (here a stationary change) in the level of isopycnal surfaces.

It follows that transitions formed with $Fr_* < Fr < Fr_c$ will be unstable. Stable jumps in the stratified flows will occur only if momentum and energy loss by upstream wave propagation is precluded from blocking and changing the upstream flow, i.e. stable jumps will only be formed in flows with $Fr \geqslant Fr_c (= 8.0$ and 4.8 for $\eta = 0$ and

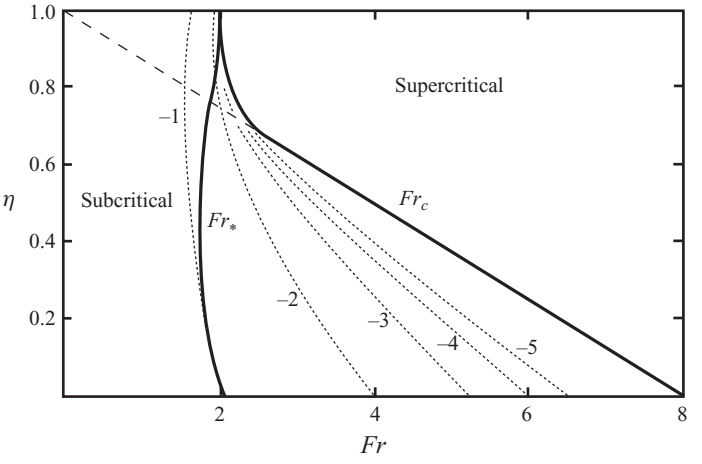

FIGURE 4. The Froude numbers Fr_c and Fr_* as functions of η for flows with η profiles. The curve Fr_c is the boundary where $c/U_1 = 0 -$ (§ 4.2). Upstream-propagating waves are possible if $Fr < Fr_c$. The curves numbered $(n =) -1, -2, \ldots, -5$, show the non-dimensionalized speeds, $-c/U_1 = 10^n$, for long upstream-travelling mode 1 waves, where U_1 is the maximum flow speed in the η profile. Long mode 2 waves also occur, but only at smaller Fr than the mode 1 waves. No internal waves or columnar modes can propagate upstream, ahead of a stationary hydraulic jump, if $Fr \geqslant Fr_c$. The curve Fr_* denotes the Froude number above which the conservation equations at a transition can be satisfied with a positive loss of energy flux (§§ 3 and 7.1(i)). Fr_* is less than Fr_c except in the two-layer case, $\eta = 1$, when the two values coincide. The dashed curve (continuing along Fr_c to the point $Fr = 8$ and $\eta = 0$) is $Fr = 8(1 - \eta)$, the value of Fr when the $\min(Ri) = 1/4$. It coincides with Fr_c when $\eta < 2/3$. The curve $Fr = Fr_c$ may be regarded as the lower boundary of Fr for the existence of 'stable' hydraulic jumps. For values of $Fr < Fr_c$ hydraulic jumps will decay through the upstream propagation of long internal waves or columnar modes. The region where stable jumps are possible, $Fr > Fr_c$, is marked 'supercritical'. Since here $\min(Ri) < 1/4$, the flow may be unstable to Kelvin–Helmholtz instability.

0.4, respectively). As is shown in § 6, the jump amplitude and loss of energy flux may be relatively large at these Froude numbers, implying that jumps may inevitably be of substantial size and cause significant mixing. The implications are discussed further in § 7.1.

5. 'Similar' and 'shape-preserving' transitions

Before engaging in a discussion in § 6 of the possible forms of flow downstream of a transition from the upstream η or cosine profiles, we return briefly to the general profiles (1) and (2) and consider the implications of assuming that the downstream profiles are similar to those upstream. This may be expected for small-amplitude transitions when the Froude number is only slightly greater than Fr_c, and will provide values for comparison with later calculations in § 6. Two distinct cases are possible, and are here distinguished by the titles 'similar' and 'shape-preserving'.

First, the upstream and downstream velocity and density profiles may be 'similar' in the sense that $F_1(x) = F_2(x)$ and $f_1(x) = f_2(x)$, thus dictating that, since $f_1(0) = 1$, the value of $f_2(1) = 1$ so and $\delta = 1$; the fluid density on the horizontal boundary is conserved through the transition.

The diapycnal fluxes within the transition region were discussed in § 2.4. The density, ρ_A, on the isopycnal surface at height $z1$ upstream and $z2$ downstream is

the same on the two sides of the transition and so, from (2), $f_1(z1/h_1) = f_2(z2/h_2)$. But $f_1(x) = f_2(x)$, and $f_1(x)$ is monotonic, and consequently $x1 = z1/h_1 = z2/h_2 = x2$. Equation (B 2) becomes $Q_A = (U_1h_1 - U_2h_2)\int_0^{x1} F_1\,\mathrm{d}x$. If there is no entrainment, $Q = 0$ (and $P = 1$), and (A 1) gives $U_1h_1 = U_2h_2$, so $Q_A = 0$. Similarly from (B 5), $F_A = 0$ in similar flows when $Q = 0$: for such flows there is no volume or mass flux across isopycnal surfaces within the transition which, lacking such diapycnal transports, cannot be regarded as being, in the usual sense, turbulent. Isopycnals simply bend and remain continuous within the rather passive transition. In 'similar' flows with no entrainment ($P = 1$), energy cannot be lost by turbulence within the transition region, only by the downstream radiation of internal waves.

Second, there are 'shape-preserving' flows in which $F_2 = F_1$ and $f_2' = f_1$ (instead of $f_2 = f_1$). In this case δ is not necessarily equal to 1; the density profile remains the same but the range of density is reduced. If also $f_1 = F_1$, as in the example profiles (27) and (30), $P_0 = 1$ and (7) gives

$$Fr = qFr_*(q^2 - P)/[2P(q - P^2)], \tag{34}$$

with $\delta = 1/P$, whilst from (8) the non-dimensional rate of loss of energy flux in the transition is

$$E = F_r \int_0^1 F_1^3\,\mathrm{d}x(1 - P^3/q^2)/2 - 2(q-1)\left[\int_0^1 xF_1^2(x)\,\mathrm{d}x + \int_0^1 F_1(x)\int_x^1 F_1(y)\,\mathrm{d}y\,\mathrm{d}x\right]. \tag{35}$$

Differentiating with respect to P, it can readily be shown that E is a maximum at $P = 1$ or (from (4)) when $\delta = 1$, for all shape-preserving transitions. (This is in accord with Appendix C. Equations for E for the η-profile and the cosine profile in shape-preserving flows are given in Appendix F. In both cases E is positive if $q > 1$, but < 0 if $q < 1$, implying that an increase in layer thickness is required for a loss in energy flux.)

We apply these results to the η profiles. Equations (34) and (35) provide relations between q, P and F_r, and between E and q, P and F_r, respectively. (For the two-layer flow given by the η profile with $\eta = 1$, with no entrainment, (34) and (35) reduce to $Fr = q(q+1)$ and $E = Fr^{1/2}(q-1)^3/2q$, respectively, which reduces to the form for a single layer flow given by Lighthill (1978) when $\Delta = 1$.) Figure 5(*a*, *b*) shows the locus of points of constant Fr in the (q–P) plane when $\eta = 0$ and 0.4, respectively, together with regions where $Fr < 0$ and $E < 0$ (excluded by conditions (*g*) and (*f*)), and the lines $\min(Ri_2) = 1/4$ and $S = 1$, corresponding to conditions (*h*) and (*i*), respectively. The maximum value of P on a line of constant Fr is given using (19) and, for example, when $\eta = 0$ is found to be

$$P_m = [(1+Fr)/3](2/Fr)^{2/3} \quad \text{when } q_m = [(1+Fr)/3](2/Fr)^{1/3}. \tag{36}$$

Evaluation of the integrals and substitution in (35) gives

$$E = Fr/8 + 5/12 - 2^{4/3}(1+Fr)/(9Fr^{1/3}), \tag{37}$$

which is positive for all $Fr \geqslant Fr_* = 2$, so giving the rate of loss of energy when the entrainment rate P is greatest. However, as seen for example in figure 5(*a*), the maximum values of P on the curves of constant Fr are in a region where $S > 1$ to the left of the line $S = 1$ where the flow is unstable to a further transition (condition (*i*)). The maximum 'allowable' values of P are where the curve $S = 1$ intersects the curves

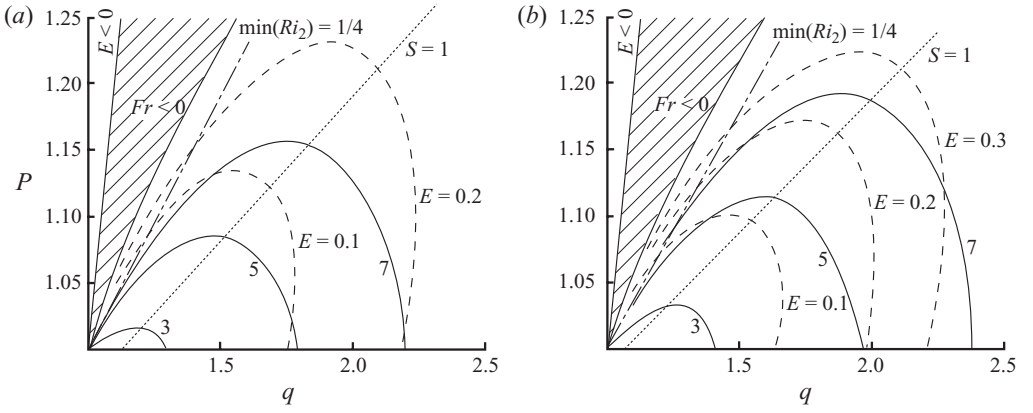

FIGURE 5. The locus of points of constant $Fr = 3$, 5 and 7 (labelled lines) and constant E (dashed lines) in the $(q–P)$ plane for shape preserving transitions with (a) $\eta = 0$ and (b) $\eta = 0.4$. $S = 1$ is shown as a dotted line and $\min(Ri_2) = 1/4$ as a dot-dash line. S is $\leqslant 1$ to the right of $S = 1$ and $\min(Ri_2) > 1/4$ is also to the right of $\min(Ri_2) = 1/4$. $Fr < 0$ in the hatched region and $E < 0$ close to the P-axis, both regions where no jumps are possible. The condition (f) for a physically possible transition (with $E \geqslant 0$) and stability conditions (h) and (i) are satisfied at relatively large values of q.

of constant Fr. (The corresponding values of P, q and E for selected Fr are plotted later in figure 7.)

But what happens when Fr becomes substantially greater than Fr_*, particularly when $Fr > Fr_c$ and when the downstream flow profiles differ from those upstream because of mixing in the transition? In the following section it should be borne in mind that when $Fr_* < Fr < Fr_c$ jumps and downstream flows are 'virtual' in the sense that transitions will collapse through the radiation of long internal waves travelling upstream. Analysis of such flows are however included to demonstrate the trends that follow the use of the conservation equations even though the solution of the Taylor–Goldstein equation (Appendix D) implies long waves will destabilize transitions.

6. Finding the downstream flow profiles

6.1. *The representation of the downstream flow*

The form of the downstream flow following a transition when $Fr > Fr_*$ is unknown, although the profiles, f_2' and F_2, must conform to the physical constraints imposed on the downstream flow. For generality we seek downstream profiles that have density and velocity profiles expressed as the sum of a linear variation in height plus terms of a truncated series of sinusoidal terms:

$$f_2'(x = z/h_2) = 1 - x + \sum_{m=1}^{m=4} a_m \sin(m\pi x) \tag{38a}$$

and

$$F_2(x = z/h_2) = 1 - x + \sum_{m=1}^{m=4} b_m \sin(m\pi x), \tag{38b}$$

which satisfy the conditions imposed in § 2.1 that $f_2'(0) = 1$, $f_2'(1) = 0$, $F_2(0) = 1$ and $F_2(1) = 0$. The constants, a_m and b_m, are to be found, subject to the conservation and other conditions, (c)–(k), listed in §§ 2.2–2.4.

The number of terms in the sine series is restricted to 4 simply to make computational time manageable. The method for seeking numerical solutions is outlined in Appendix G.1. For q and Fr slightly in excess of 1 and Fr_*, respectively, the downstream profiles are likely to be similar to those upstream, as suggested in § 5. The magnitude of the constants, a_m and b_m, $m = 1$–4, when the series (38) are fitted to the η and cosine upstream profiles, (27) and (30), respectively, and their goodness of fit, are discussed in Appendix G.2. The four-term sine series provides a fairly good fit to the given profiles when $\eta \leqslant 0.7$, and provides an indication of the magnitudes expected of the constants when Fr is near Fr_*.

We shall examine the forms of the downstream flow for η profile upstream flows with $\eta = 0$ and 0.4, and for the cosine profile corresponding to $\eta = 0.4$. As mentioned in § 2.5, downstream flows are to be sought for specified upstream flows at extreme values of q, P and E. For selected η and Fr and a downstream flow satisfying the conservation and other conditions, (7) provides a relation between Fr, q and P, or a relation between q and P at specified Fr. Extreme values of, say, q at constant Fr can be found by varying P. Variation of the downstream profiles (tested to ensure they satisfy the imposed conditions – Appendix G.1) may then be made to find those corresponding to extreme values of q for fixed Fr, e.g. $\min(q)|_{\eta, Fr = \text{const}}$, for the given upstream flow and calculated over the physically possible range of P and for all physically possible downstream flows. Downstream profiles giving extreme values of P, e.g. $\max(P)|_{\eta, Fr = \text{const}}$, can similarly be found. The variation of the loss in energy flux E is found through (8) which relates E to Fr, q and P. Using (7) at specified Fr, (7) and (8) provide an expression for E in terms of either q or P. Again, extreme values and corresponding downstream profiles, this time of E at given Fr, can be found by first setting P and determining q in terms of a constant Fr by (7), hence E from (8) subject to the imposed conditions, then by varying the downstream flow to give, e.g. $\max(E)|_{\eta, Fr = \text{const}}$. The particular cases chosen for examination at selected values of Fr are where

(i) the loss in energy flux E is greatest: $\max(E)|_{\eta, Fr = \text{const}}$;
(ii) the entrainment parameter P is greatest: $\max(P)|_{\eta, Fr = \text{const}}$;
(iii) the jump amplitude q is smallest: $\min(q)|_{\eta, Fr = \text{const}}$; and
(iv) the loss of energy flux is greatest but there is no entrainment:

$$\max(E)|_{\eta, Fr = \text{const}, P = 1};$$

where in each case the optimal downstream flow must satisfy the imposed conditions. Other extreme cases might be chosen, but these four are useful for comparative purposes and to allow a brief examination of the forms of possible downstream flow, at least where solutions have been found. Some of the main features characterizing the downstream flow are described in the following sections and related figures. Comparisons are made with the values estimated for shape preserving and for 'similar' downstream flows no entrainment and no mixing within the transition region that are described in § 5. We begin with the downstream flow resulting from an upstream flow specified by (27), an η profile, with $\eta = 0$.

6.2. *Downstream flows with* $\eta = 0$ *upstream* ($Fr_* = 2.0$, $Fr_c = 8.0$)

Figure 6 shows the profiles of density (f_2') and velocity (F_2) at four values of Fr extending to a value $> Fr_c$, when $\eta = 0$ in the four extreme cases. Although identical in the upstream flow, the downstream density and velocity profiles are different from one another. In the upstream profiles (shown at the left of each part of the figure) the gradients in the moving layer are uniform, but in cases (i), (ii) and (iv) the

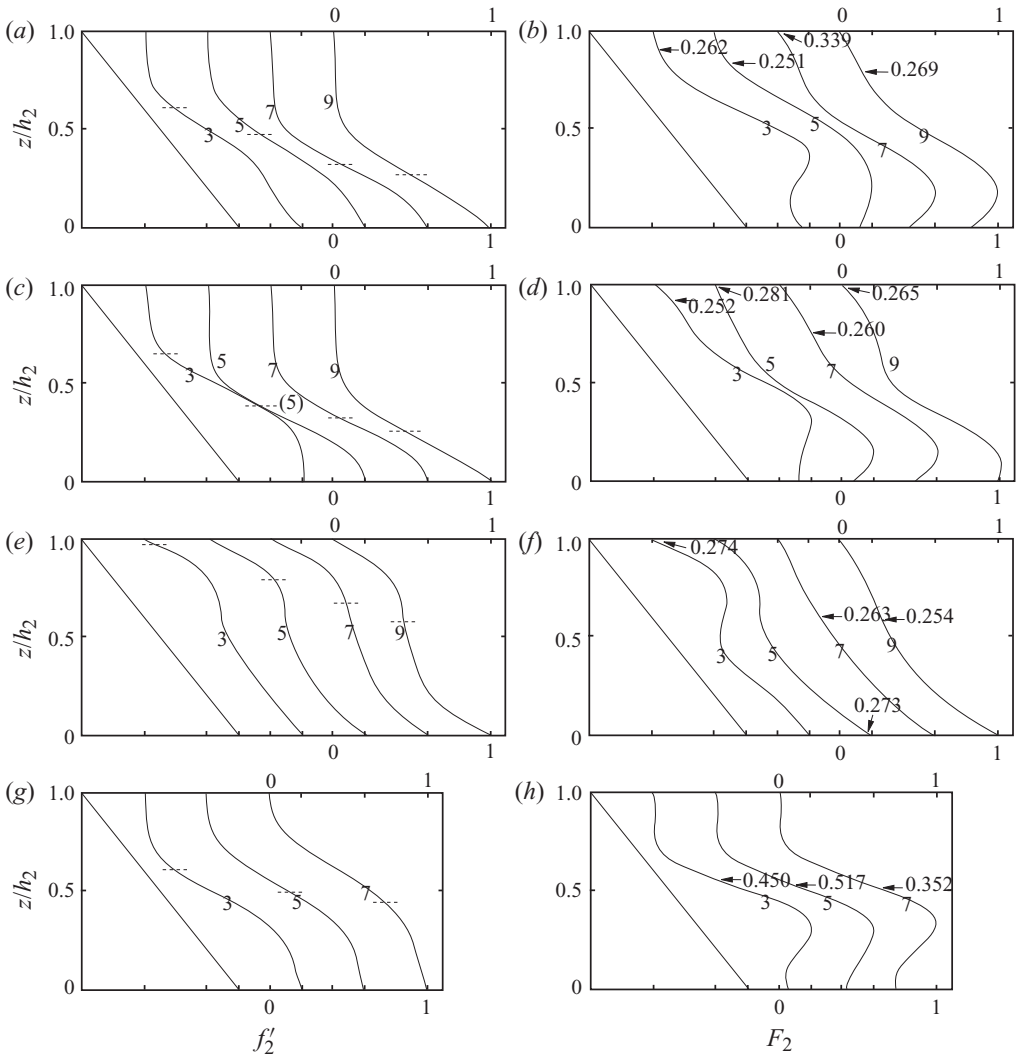

FIGURE 6. The profiles of downstream density (f_2' (*a*, *c*, *e*, *g*)) and velocity (F_2 (*b*, *d*, *f*, *h*)) at $Fr = 3$, 5, 7 and 9 when $\eta = 0$, in (*a*, *b*) case (i): E is maximum at the selected Fr; (*c*, *d*) case (ii): P is greatest; (*e*, *f*) case (iii): q is minimum; and (*g*, *h*) case (iv): E is greatest subject to $P = 1$ (no entrainment; there is no solution at $Fr = 9$ in this case). The upstream profile (but plotted as a function of z/h_1) is at the left of each set of profiles. The height of the upstream flow, $q^{-1} = h_1/h_2$, is marked by dashed lines on the f_2' profiles; q is shown in figure 7(*a*). The profiles of F_2 are normalized by dividing by the maximum value, and values of U_2/U_1, the ratio of the downstream to upstream flows at $z = 0$, are given in table 1. (The ratio of the corresponding relative densities at $z = 0$ is δ, given in figure 7*d*.) Arrows on the velocity (F_2) curves show the location and value of the minimum Richardson number, $\min(Ri_2)$.

overall tendency in the downstream flow is towards the development of a two-layer structure, most pronounced in case (iv), whilst in case (iii) the gradients are reduced at $z/h_2 \sim 0.6$, enhanced above, and remain almost unchanged near $z/h_2 = 0$. The density downstream of the transition near the horizontal boundary at $z/h_2 = 0$ is less than that upstream because $\delta < 1$, as will be seen in figure 7(*d*). The profiles of velocity F_2 are normalized by dividing by the maximum value, and values of U_2/U_1, the ratio of

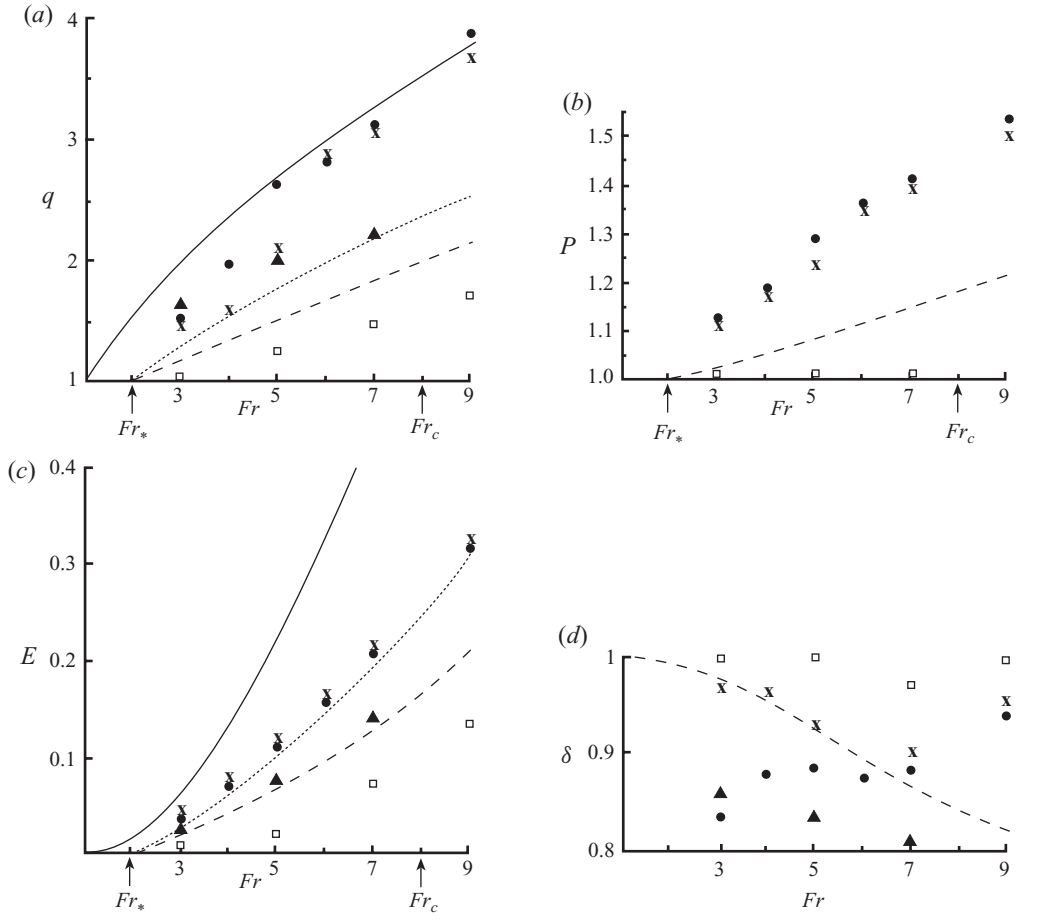

FIGURE 7. Values of (*a*) q, (*b*) P, (*c*) E and (*d*) δ, when $\eta = 0$. The points at selected Fr represent: **x** – case (i), E is maximum; ● – case (ii), P is greatest; □ – case (iii), q is smallest; ▲ – case (iv), E is maximum subject to $P = 1$ (no entrainment). The limiting Froude numbers, $Fr_* = 2.0$ and $Fr_c = 8.0$, are indicated. The dashed lines correspond to shape-preserving transitions when P is maximum. The dotted lines correspond to 'similar' upstream to downstream flow transitions when $P = 1$; and the full lines are values for the corresponding two-layer flow (illustrated in figure 3*a*) with $P = 1$. The uncertainty in Fr is ± 0.01 (Appendix F.1) and uncertainties in q, P, E and δ are about 0.1, 0.01, 0.001 and 0.1, respectively, values determined by variation in the coefficients a_m and b_m by their level of uncertainty, 0.01.

the downstream to upstream flows at $z = 0$, are given in table 1. The interested reader will observe a number of physical processes involved in the transition. For example, the region of uniform density, $f_2' \sim 0$ at $z/h_2 > 0.6$, in cases (i) and (ii), figures 6(*a*, *c*), respectively, is fluid that has been entrained from the overlying layer and which, downstream of the jump, is in motion; $F_2 > 0$.

No downstream flow satisfying the flux condition (*k*) has been found when $Fr = 9$ and when there is no entrainment (case (iv)); no values of Γ exceed 0.185. (A similar result, but settling in at a lower Fr, is found when $\eta = 0.4$: § 6.3.) Entrainment appears 'inevitable' for flows with relatively large Fr in conditions in which all the dissipation of energy flux must occur within a transition. (As noted in § 5, there is a solution at $P = 1$, with no entrainment, when the downstream flow is similar in form to that

Fr	Case ($\eta = 0$)	U_2/U_1 ($\eta = 0.4$)	U_2/U_1 (cosine; $\eta = 0.4$)	U_2/U_1 ($\eta = 0.4$)	$q_{1/2}$ ($\eta = 0.4$)	q
3	(i)	0.592	0.801	0.700	1.26	1.54
5	(i)	0.442	0.584	0.595	1.50	2.10
7	(i)	0.361	0.602	0.584	1.62	3.44
9	(i)	0.329				
3	(ii)	0.554	0.839	0.786	1.22	1.50
5	(ii)	0.450	0.640	0.609	1.44	2.14
7	(ii)	0.387	0.605	0.582	1.62	3.44
9	(ii)	0.421				
3	(iii)	0.929	0.936	–	1.29	1.20
5	(iii)	0.933	0.873	–	1.66	1.47
7	(iii)	0.848	0.834	–	1.88	1.80
9	(iii)	0.816				
3	(iv)	0.517	0.603	0.609	1.40	1.36
5	(iv)	0.401	0.463	0.465	1.96	1.76
7	(iv)	0.338	No solution	0.418	No solution	No solution
9	(iv)	No solution	No solution	No solution	No solution	No solution

TABLE 1. The ratios, U_2/U_1, of the downstream to upstream flows at $z = 0$ and at various Fr in the extreme cases (i)–(iv) defined in § 6.1, and the ratio of the downstream and upstream heights of the central isopycnal, $q_{1/2}$, defined in § 6.3 when $\eta = 0.4$. Values of $q = h_2/h_1$, are given for comparison. 'No solution' mean that no solutions are found that satisfy condition (k): $\Gamma \sim 0.2$.

upstream, but in this case the transition is not turbulent and energy cannot be lost through mixing within the transition region, only through the radiation of internal waves.)

Values of S and the coefficients a_i and b_i in (38) for the respective downstream flows are given in table 2. In cases (i) and (ii) the extreme flows are generally close to the limit imposed by condition (h), with $\min(Ri_2)$ near 0.25, the smallest values of Ri_2 (marked on the F_2 profiles) being towards the top of the flowing region where entrainment is evident. In some cases (e.g. case (i) at $Fr = 3$ and case (iii)) the table shows S is also close to its bounding value of unity imposed by condition (i). Relaxation of condition (h) (that of $\min(Ri_2) \geqslant 1/4$) leads to downstream flows with larger rates of loss of energy flux, and with condition (i) ($S \leqslant 1$) generally providing a limiting constraint. When there is no entrainment (case (iv); figure 6h), the downstream flow has a pronounced shear layer at the mid-depth ($z/h_2 \sim 0.5$) and signs of a jet-like structure below. $\min(Ri_2)$ is substantially greater than 0.25 and $S < 1$; the flux conditions (j) and (k) then provide limiting constraints. (The effect of the flux conditions is made evident in comparing the solutions for the downstream flows with and without these conditions. Although the removal has a relatively small effect on the density profiles, it results in more uniform slopes in the velocity below $z = h_2$ in case (i), and in case (ii) low shear layers develop at mid-depth. In case (iv), the downstream flows have $\min(Ri_2)$ near 0.25 and S is substantially less than unity in the absence of the flux conditions: it is condition (h) that provides a limiting control on the downstream flows.)

The coefficients, a_m and b_m, in table 2 for $\eta = 0$ generally decrease in magnitude as m increases, suggesting convergence, but in some case (e.g. for $|a_m|$ in case (iii) and for b_m in case (iv)) values with $m = 2$ exceed those with $m = 1$, the larger second harmonic

Fr	Case	η/cos	S	a_1	a_2	a_3	a_4	b_1	b_2	b_3	b_4
3	(i)	0.0	0.99	−0.12	0.12	−0.02	−0.03	0.26	0.15	−0.11	−0.045
5	(i)	0.0	0.89	−0.19	0.11	0.025	−0.005	0.27	0.17	−0.045	0.015
7	(i)	0.0	0.89	−0.325	0.06	0.075	0.02	0.175	0.24	0.09	−0.01
9	(i)	0.0	0.84	−0.37	0.01	0.04	0.01	0.18	0.225	0.07	0
3	(ii)	0.0	0.96	−0.025	0.20	0.02	−0.03	0.26	0.15	−0.005	−0.06
5	(ii)	0.0	0.90	−0.31	0.08	0.08	0.02	0.03	0.18	0.10	0.02
7	(ii)	0.0	0.89	−0.325	0.06	0.075	0.02	0.10	0.16	0.105	0.02
9	(ii)	0.0	0.90	−0.41	−0.03	0.03	0.01	−0.08	0.06	0.01	0.025
3	(iii)	0.0	0.98	0.08	−0.10	0.06	−0.02	0.02	−0.14	0.09	0
5	(iii)	0.0	0.97	0.06	−0.14	0.045	−0.02	−0.13	−0.09	0.045	−0.02
7	(iii)	0.0	1.00	0.06	−0.14	0.02	−0.03	−0.15	−0.03	−0.01	−0.01
9	(iii)	0.0	0.98	−0.015	−0.165	0.01	−0.03	−0.18	−0.06	−0.01	−0.01
3	(iv)	0.0	0.77	−0.06	0.175	0.01	−0.03	0.16	0.32	−0.05	−0.10
5	(iv)	0.0	0.62	0	0.16	−0.01	−0.015	0.185	0.34	−0.035	−0.085
7	(iv)	0.0	0.56	0.105	0.115	−0.05	0	0.30	0.36	−0.10	−0.11
9	(iv)	0.0	No solution								
3	(i)	0.4	0.88	0.125	0.17	−0.04	−0.01	0.20	0.07	−0.04	0.02
5	(i)	0.4	0.86	0.025	0.19	0.02	−0.04	0.355	0.05	−0.03	−0.06
7	(i)	0.4	0.90	−0.275	0.10	0.095	0.025	−0.04	0.035	0.08	0.035
3	(ii)	0.4	0.96	0.125	0.17	−0.04	−0.01	0.175	0.055	−0.02	0.03
5	(ii)	0.4	0.92	−0.03	0.18	0.04	−0.035	0.215	0.07	0.035	−0.05
7	(ii)	0.4	0.97	−0.29	0.09	0.10	0.03	−0.06	0.03	0.095	0.045
3	(iii)	0.4	0.96	0.34	−0.01	0.01	−0.01	0.18	0.04	0.04	−0.03
5	(iii)	0.4	1.00	0.27	−0.03	0.08	−0.05	0.06	0.10	0.045	−0.025
7	(iii)	0.4	0.95	0.21	−0.045	0.07	−0.03	−0.04	0.10	0.035	0
3	(iv)	0.4	0.69	0.34	0.025	−0.05	0.01	0.60	0.015	−0.14	0.11
5	(iv)	0.4	0.50	0.36	−0.075	0	0.01	0.62	0.04	−0.12	0.125
7	(iv)	0.4	No solution								
3	(i)	cos	0.96	0.125	0.17	−0.04	−0.01	0.40	0.055	−0.07	0.045
5	(i)	cos	0.90	0.025	0.17	0.02	−0.03	0.355	0.02	−0.02	−0.03
7	(i)	cos	0.92	−0.275	0.10	0.095	0.025	0.005	0.055	0.05	0.015
3	(ii)	cos	0.96	0.025	0.20	−0.02	−0.04	0.175	0.115	−0.04	−0.035
5	(ii)	cos	0.91	−0.075	0.17	0.05	−0.025	0.215	0.10	0.055	−0.045
7	(ii)	cos	0.94	−0.29	0.09	0.10	0.03	−0.015	0.05	0.085	0.035
3	(iv)	cos	0.66	0.28	0.05	−0.05	0.02	0.52	0.045	−0.14	0.07
5	(iv)	cos	0.47	0.315	−0.045	−0.02	0.02	0.575	0.00	−0.11	0.135
7	(iv)	cos	0.48	0.415	−0.13	0.02	0	0.545	0.12	−0.80	0.095

TABLE 2. Values of the jump stability factor S and the coefficients a_m, b_m in (38), for the upstream η profiles (with $\eta = 0$ and 0.4) and the cosine profile (cos) equivalent to $\eta = 0.4$ and at various Fr in the extreme cases (i)–(iv) defined in § 6.1. 'No solution' means that no solutions are found that satisfy condition (k): $\Gamma \sim 0.2$.

being required to represent the substantial changes from the uniform gradients of the upstream profiles as flow passes through a transition.

Figure 7 shows values of q, P, E and δ at several values of Fr in the extreme cases, together with values for 'similar' upstream and downstream flows with $P = 1$ (when there is no entrainment and no mixing in the transition region as shown in § 5) and for shape-preserving transitions when the entrainment, given by P, is maximum (subject to $S \leqslant 1$; see § 5 and figure 5a). As in single-layer flows, values of the jump amplitude q and the rate of loss of energy flux E increase with Fr in each case. The 'similar' and shape preserving transitions underestimate the possible jump amplitudes and rates of energy loss. The values of q and E in the corresponding two-layer flow

(illustrated in figure 2*a*) are shown for comparison in figure 7(*a*, *c*). The rates of loss of energy flux, E, for the equivalent two-layer flows overestimate those of the $\eta = 0$ flows.

Entrainment P increases with Fr (figure 7*b*). Values of P in case (ii) are the greatest that can be found consistent with the applied conditions, and these are generally only slightly larger than those in case (i) (maximum E) and within 0.5 % of P_m. There is no entrainment or mixing in the two-layer flow and, in this case, $P = 1$ in figure 7(*b*) and $\delta = 1$ in figure 7(*d*). There is relatively little entrainment when the jump amplitude, q, is minimized (case (iii)). The relative reduction in density, δ, at $z = 0$ caused by mixing in the transition region, decreases as Fr increases from 3 to 7 in case (i) (and in case (iv)) and then increases at $Fr = 9$, but is smaller – indicating more mixing – in case (ii), lying between 0.8 and 0.9 when $Fr = 3$–7. (Removal of the flux condition results in solutions for the downstream flow with larger rates of loss of energy flux E and greater entrainment rates P, but relatively little change in jump amplitudes q.)

Figure 8 shows the non-dimensional diffusive flux, F given by (B 7), and the advective flux, Q_* given by (B 3), across the 10 selected isopycnal surfaces, $f_1 = (1 - 0.1n)$, $n = 1$, 10, marked in figure 3, as they pass through the transition region. The non-dimensionalized (positive) diffusive fluxes increase with Fr. The diffusive flux tends to zero at the bottom (through which there can be no flux) and at the top of the flowing layer. The upward non-dimensional advective flux is equal to $(1 - P)$, which is $\leqslant 0$, at isopycnal level $n = 10$ marking the top of the flowing layer. In case (iii), $P = 1$ and the flux is zero at isopycnal level 10, and the diapycnal flux is very close to zero above level 7. The advective fluxes are generally positive at level 1 near the horizontal plane and change sign at level $n = 4 \pm 2$. As noted in regard to figure 7, $\delta < 0.9$ for $Fr = 3$–7 in case (ii) and there is no isopycnal surface, $n = 1$, with $f_1 = 0.9$, downstream. Mixing of the relatively dense fluid in the near-bottom region with that above it results in a decrease of its density within the transition, and the advective flux in the upstream flow must all pass upwards through the isopycnal surface in the transition region. As a result, the 'non-dimensional' advective fluxes in figure 7(*b*) (right) for $Fr = 3$, 5 and 7 are equal at level $n = 1$. Both F and Q_* are relatively small for $Fr = 3$ and 5 at $n = 1$ (or near $z = 0$) in case (iii); the density profiles (figure 6*c*) remain similar to those upstream and $\delta \sim 1$ (figure 7*d*).

We now examine the downstream flow when the upstream flow is specified by (22) with $\eta = 0.4$ in which the density and velocity are uniform below the level $z/h_1 = 0.4$.

6.3. *Downstream flows with* $\eta = 0.4$ *upstream* ($Fr_* = 1.73$; $Fr_c = 4.8$)

The downstream density and velocity profiles when $\eta = 0.4$ are shown in figure 9 with Fr extending to values $> Fr_c$. Although still reflecting the uniformity of the upstream flow below $z/h_1 = \eta$, the general trends are like those at $\eta = 0$ (figure 6). The case (i) and (ii) curves are similar to one another. The density profiles have a two-layer structure with relatively uniform regions near $z/h_2 = 0$ and $z/h_2 = 1$, and a central region of higher gradient that becomes closer to the horizontal boundary as Fr increases. As seen in figure 10(*d*), however, δ is close to unity implying, from (4), that $P \approx P_0$ and, unlike the case when $\eta = 0$, mixing does not reduce the density at $z = 0$ by more than 0.1 %; in this case there is a layer of uniform density in the upstream flow adjoining the boundary at $z = 0$ that is not totally eroded in the transition. The velocity profiles are less regular than the density whilst maintaining a relatively low gradient near $z/h_2 = 0$ and a shear near $z/h_2 = 1$ where Ri_2 has its lowest values, near 0.25. Values of S given in table 2 are significantly less than unity, implying that generally the condition (*h*) of dynamical stability limits the extreme downstream flow rather than

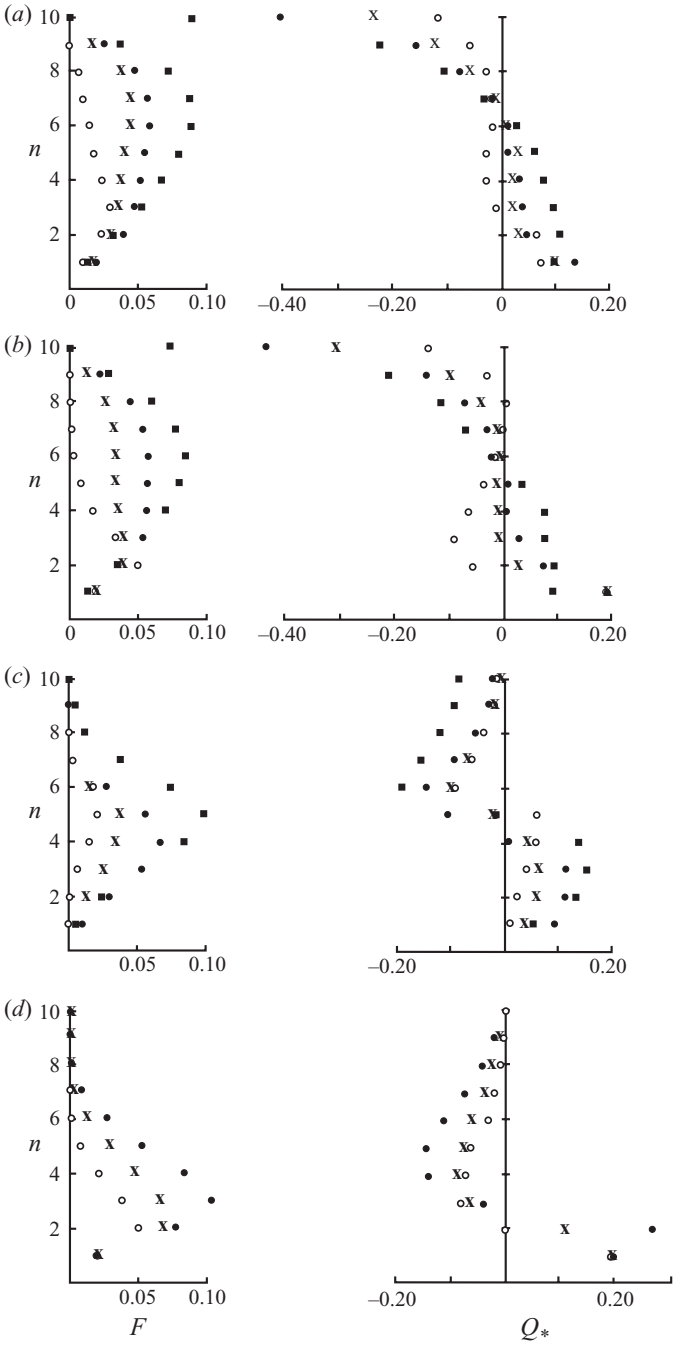

FIGURE 8. The non-dimensional upward diffusive and advective diapycnal fluxes, F and Q_*, given by (B 7) and (B 3), respectively, across the 10 selected isopycnal surfaces (numbered from $n = 1$, the lowest, to $n = 10$ at $z = h_i$) which are marked as dots in figure 3(a), as they pass through the transition region when $\eta = 0$. (a) case (i); (b) case (ii); (c) case (iii); and (d) case (iv). The fluxes are shown at: o, $Fr = 3$; x, $Fr = 5$; ●, $Fr = 7$; and ■ $Fr = 9$. The upward advective flux Q_* at the upper ($n = 10$) isopycnal is equal to $(1 - P)$. The uncertainty in the flux values is about 0.01.

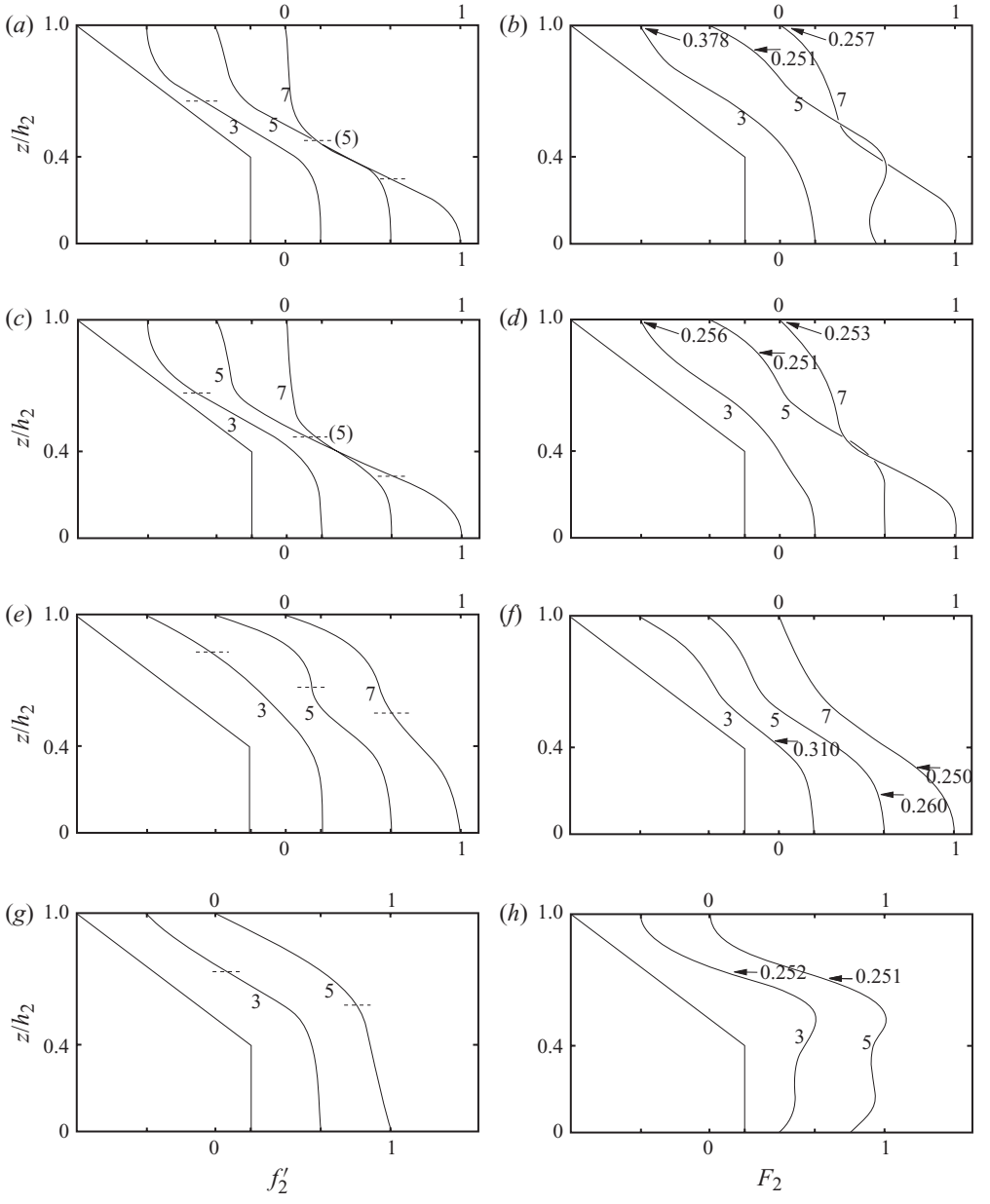

FIGURE 9. The profiles of downstream density (f_2' (*a*, *c*, *e*, *g*)) and velocity (F_2 (*b*, *d*, *f*, *h*)) at $Fr = 3$, 5 and 7 when $\eta = 0.4$, in (*a*, *b*) case (i): E is maximum at the selected Fr; (*c*, *d*) case (ii): P is greatest, (*e*, *f*) case (iii): q is minimum and (*g*, *h*) case (iv): E is greatest subject to $P = 1$ (no entrainment). The upstream profile (but plotted as a function of z/h_1) is at the left of each set of profiles. The height of the upstream flow, $q^{-1} = h_1/h_2$, is marked by dashed lines on the f_2' profiles; q is given in figure 10(*a*) and table 1. The profiles of F_2 are normalized by dividing by the maximum value, and values of U_2/U_1, the ratio of the downstream to upstream flows at $z = 0$, are given in table 1. (The ratio of the corresponding relative densities at $z = 0$ is δ, given in figure 10*d*.) Arrows on the velocity (F_2) curves show the location and value of the minimum Richardson number, $\min(Ri_2)$. As mentioned in § 4.2, the minimum upstream Ri is $<1/4$ if $Fr > 4.8$.

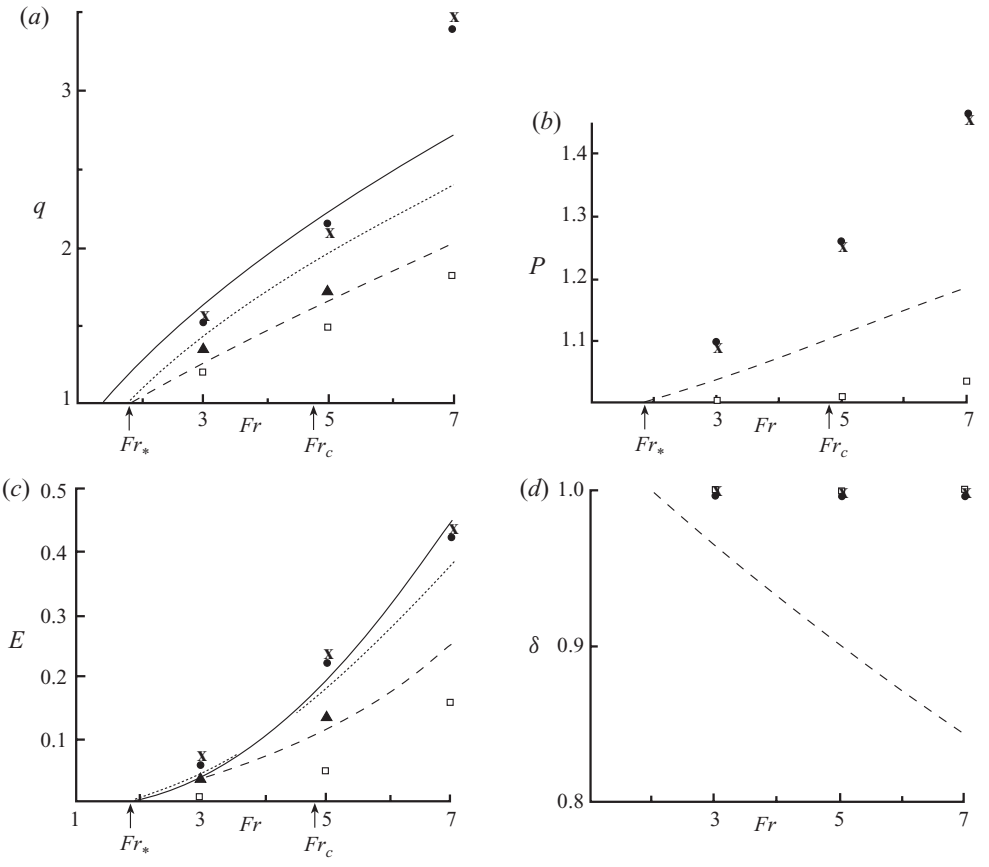

FIGURE 10. Values of (*a*) q, (*b*) P, (*c*) E and (*d*) δ, when $\eta = 0.4$. The points at selected Fr represent: **x** – case (i), E is maximum; ● – case (ii), P is greatest; □ – case (iii), q is smallest; and ▲ – case (iv), E is maximum subject to $P = 1$. The limiting Froude numbers, $Fr_* = 1.73$ and $Fr_c = 4.8$, are indicated. The dashed lines correspond to shape-preserving transitions when P is maximum. The dotted lines correspond to 'similar' upstream to downstream flow transitions when $P = 1$; and the full lines are values for the corresponding two-layer flow (illustrated in figure 3*b*) with $P = 1$. The uncertainties in values are as given in the caption of figure 7.

the condition (i) of no possible further transition. (Case (i) with $Fr = 3$ is an exception: neither Ri_2 nor S are near their limits of 1/4 and 1. This is true even if the diapycnal flux conditions (*j*) and (*k*) are removed. A jet-like structure develops in the upper part of the layer when $Fr = 7$ and when the constraint (*h*), $\min(Ri_2) \geqslant 1/4$, is removed.)

At $Fr = 3$, the profiles of case (iii) are not dissimilar from those upstream, but the density becomes more uniform at $z/h_1 \sim 0.6$, and the region of higher velocity more confined near $z = 0$ at higher Fr.

The height of the isopycnal with the mean density, that with $f_1 = 0.5$, at the centre of the upstream density gradient, is $h_1(1 + \eta)/2$. Downstream, the isopycnal is at $f_2 (\approx f_2' \text{ since } \delta \approx 1) = 0.5$. Its height can be found from the profiles of figure 9. The ratio of the downstream and upstream heights, $q_{1/2}$, of this isopycnal is given in table 1 and, like q, increase with Fr. Since, moreover, there is a lack of symmetry of the downstream profiles of density and velocity, f_2' and F_2, respectively, about their values of 0.5 in the moving layer, in each of the four cases the mixing that occurs in the transitions is not symmetrical as in Kelvin–Helmholtz instability at a stratified

interface between two deep layers. Mixing in the transition is not localized to the region of density gradient and velocity shear, but is affected by the presence of the boundary at $z = 0$.

As mentioned in § 6.2, no downstream flow satisfying the flux condition (k) has been found in case (iv) when $Fr = 7$ or 9 when there is no entrainment; there are no values of Γ that exceed 0.15 and 0.092 when $Fr = 7$ and 9, respectively, and entrainment appears inevitable at these values of Fr. At $Fr = 3$ and 5, the density profiles in case (iv) (figure 9g) remain broadly similar to the upstream profiles with an upper region of gradient but with a relatively deeper lower uniform region. The velocities have similar forms but with greater evidence of higher harmonics; the b_3 coefficients in table 2, although substantially less than b_1, are larger than in other cases. In each case the parameter S is less than unity but $\min(Ri_2) \sim 0.25$ in the region of high shear and density gradient; condition (h) limits the extreme downstream flow. The exception is case (iii) where both S and $\min(Ri_2)$ appear to provide limits to the possible downstream flows.

The variation of q, P and E with Fr (figure 10a–c) shows trends similar to those for $\eta = 0$, but the range of E is substantially increased, and the two-layer approximation provides more representative values for cases (i) and (ii). In the lower values of Fr, the 'similar' downstream profile with $P = 1$ provides an approximate guide to the values of q and E, although not to P. Except for the shape preserving transition when P is maximum, $\delta \approx 1$ in figure 10(d); the density at $z = 0$ remains close to its upstream value in $z/h_1 \leqslant \eta$.

The non-dimensional diapycnal fluxes are shown in figure 11. These have values comparable to those in figure 8 for $\eta = 0$. The greatest difference is because there is an upstream near-boundary layer of uniform density which is not completely eroded in the transition when $\eta = 0.4$; the density near $z = 0$ is only slightly reduced in the transition ($\delta \approx 1$). Consequently although there is an upward advective flux Q_* through the isopycnal at level $n = 1$, this isopycnal does survive in the transition and emerges in the downstream flow when $\eta = 0.4$.

6.4. *Downstream flows of cosine form corresponding to* $\eta = 0.4$

Figures 12–14 show the functions and values for the upstream cosine profiles of density and velocity (30) corresponding to figures 9–11 when $\eta = 0.4$ and $Fr > Fr_* = 1.83$. (Case (iii) is not shown. The other cases are sufficient to demonstrate the main conclusion, one of similarity to the upstream η profiles.) The values, Fr, q and E, are taken to be those equivalent to flows with $\eta = 0.4$, for easy comparison, e.g. q in figure 13(a) is equal to h_2/h_1, not h_2/h_1'.

The density and velocity profiles (figure 12) are very similar to those of figure 9: the discontinuities in density and velocity gradients of the η profiles, absent in the cosine profiles, make little difference to the shape of the downstream flows. An exception is that, in case (iv), there is a solution at $Fr = 7$. (In this case, the density of the downstream flow at the boundary, $z = 0$, proportional to δ, is substantially less than unity (figure 13d), implying that internal mixing has reduced the density.) No solution has been found, however, with $\Gamma > 0.12$ when $Fr = 9$. Condition (k) is failed, again supporting the notion that transitions at large Fr must involve entrainment. With this exception, the values of q, P and E displayed in figure 13(a–c), are similar to those of the corresponding figure 10, and the diapycnal fluxes F and Q_* are also similar (figure 14); the discontinuities in the η profile make little difference to the amplitude of the hydraulic jump, to the loss in energy flux or to the diapycnal fluxes within the transition region.

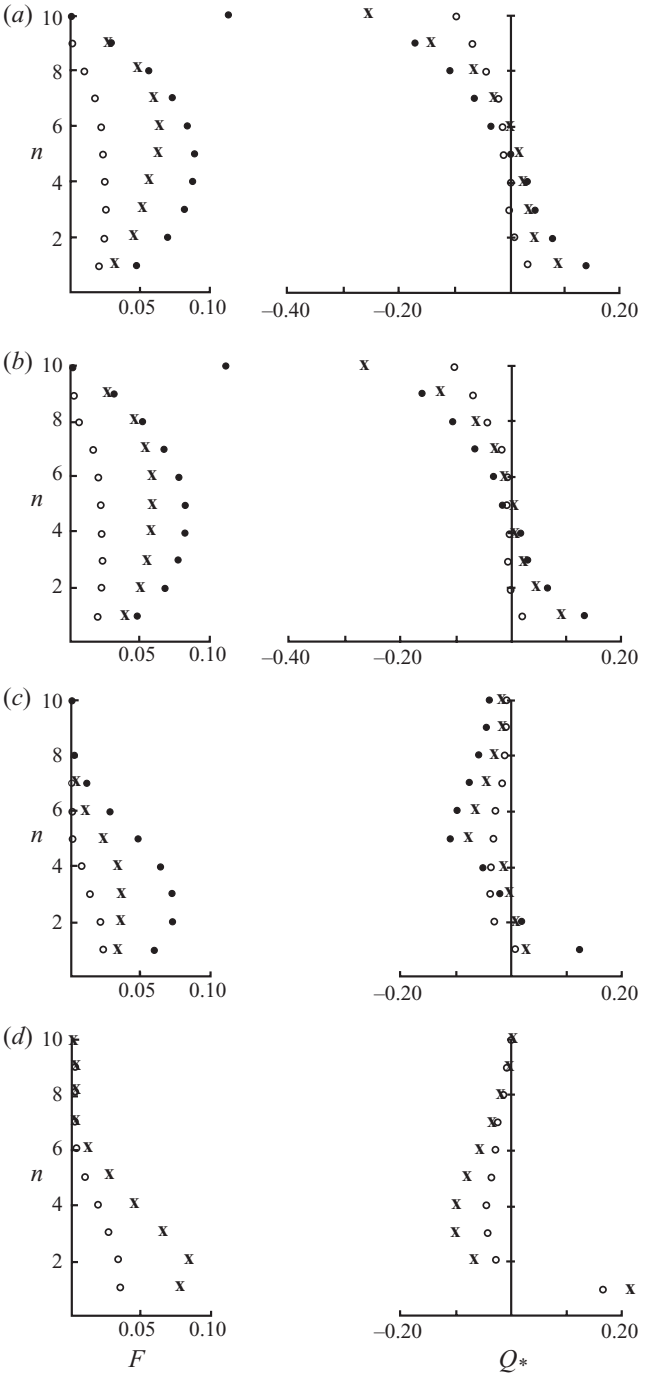

FIGURE 11. The non-dimensional upward diffusive and advective fluxes, F and Q_*, given by (B 7) and (B 3), respectively, across the 10 selected isopycnal surfaces (numbered from $n = 1$, the lowest, to $n = 10$ at $z = h_i$) which are marked in figure 3(b), as they pass through the transition region when $\eta = 0.4$. (a) case (i); (b) case (ii); (c) case (iii); (d) case (iv). The fluxes are shown at: **o**, $Fr = 3$; **x**, $Fr = 5$; and ●, $Fr = 7$. The upward advective flux Q_* at the upper isopycnal ($n = 10$) is equal to $(1 - P)$. The uncertainty in the flux values is about 0.01.

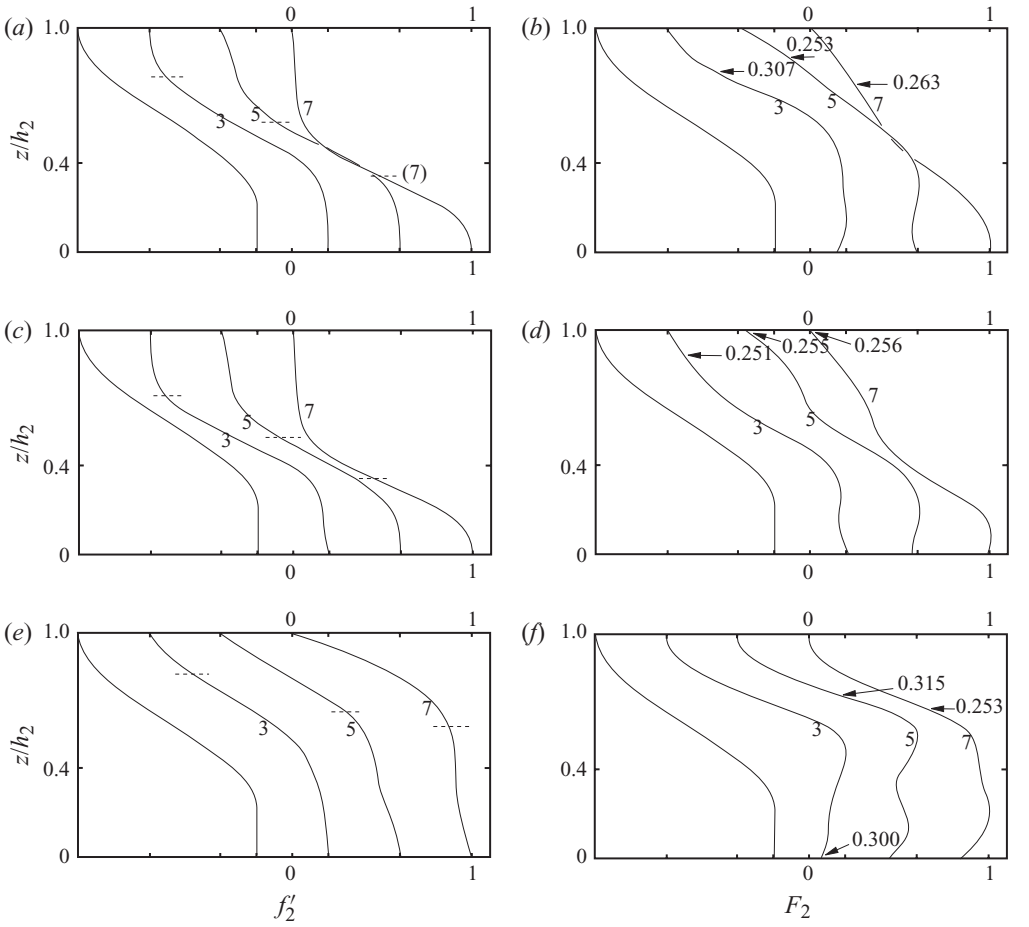

FIGURE 12. The profiles of downstream density (f_2' (a, c, e)) and velocity (F_2 (b, d, f)) at $Fr = 3$, 5 and 7 for the cosine upstream flow equivalent to the η profile when $\eta = 0.4$, in (a, b) case (i): E is maximum at the selected Fr; (c, d) case (ii): P is greatest and (e, f) case (iv): E is greatest subject to $P = 1$ (no entrainment). (Case (iii) is not shown.) The upstream profile (but plotted as a function of $y_1 = z/h_1'$ as defined in (31)) is at the left of each set of profiles. The height of the upstream flow, $q^{-1} = h_1'/h_2$, is marked by dashed lines on the f_2' profiles; q is shown in figure 13(a). The profiles of F_2 are normalized by dividing by the maximum value, and values of U_2/U_1, the ratio of the downstream to upstream flows at $z = 0$, are given in table 1. (The ratio of the corresponding relative densities at $z = 0$ is δ, given in figure 13d.) Arrows on the velocity (F_2) curves show the location and value of the minimum Richardson number, $\min(Ri_2)$.

7. Conclusion

7.1. *Discussion of results*

We have examined and compared the downstream profiles of density and velocity and the related parameters (q, P, E and δ) and diapycnal fluxes (F and Q_*) for hydraulic transitions, taking as particular examples those occurring in the upstream flows shown in figure 3 and defined by (27), with $\eta = 0$ and 0.4, and (30) with $\eta = 0.4$, under a set of conditions ((*c*)–(*k*)) relating to continuity, to stability and to mixing within the transition, to which the downstream flow must conform to be physically realistic. The main findings and implications are as follows:

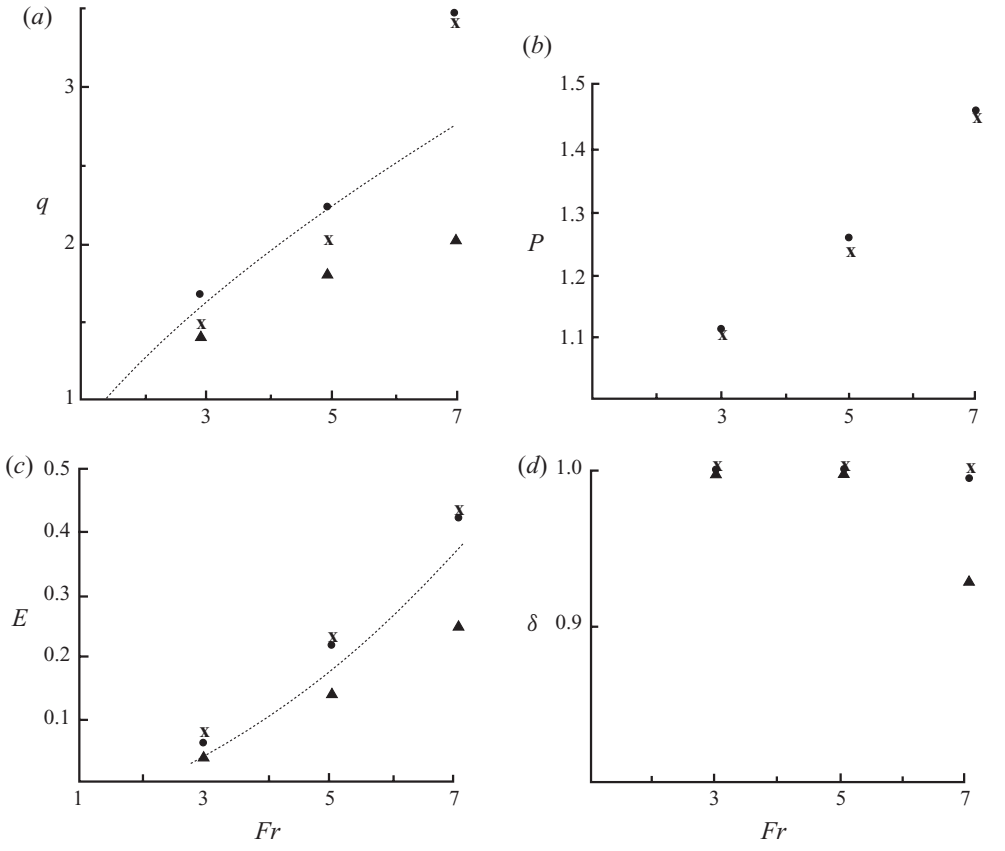

FIGURE 13. Values of (*a*) q, (*b*) P, (*c*) E and (*d*) δ, for the cosine upstream flow equivalent to the η profile when $\eta = 0.4$. At selected Fr, the points represent: **x** – case (i), E is maximum; ● – case (ii), P is greatest; ▲ – case (iv), E is maximum when $P = 1$. (Case (iii) is not shown.) The dotted lines correspond to 'similar' upstream to downstream flow transitions when $P = 1$. The uncertainties in values are as given in the caption of figure 7.

(i) A Froude number Fr_* is determined in §3 by applying the conditions of conservation of volume, mass and momentum fluxes across a transition with $q = 1$ (no change in isopycnal levels) and $P = 1$ (when there is no entrainment). The value of Fr_* is consistent with interpolation to $q = 1$ and $P = 1$ of the values of q, P and E at higher Fr shown in figures 7, 10 and 13: the maximum loss in energy flux, E, tends to zero as Fr tends to Fr_*.

(ii) Solution of the Taylor–Goldstein equation for the η profile (Appendix E) reveals that long internal waves can travel upstream if (and only if) Fr is less than a value Fr_c that lies at the boundary of possible dynamical stability where $\min(Ri_1) = 1/4$ when $\eta < 2/3$, but it is within the region $\min(Ri_1) < 1/4$ when $2/3 < h \leqslant 1$. As shown in figure 4, however, $Fr_* \leqslant Fr_c$, there being equality only in the two-layer case, $\eta = 1$. (Relative values of Fr_* and Fr_c are considered for other profiles in Appendix H.) Fr_c is a critical value in the sense of being the smallest Froude number at which jumps can form and remain stable. If a jump were formed in a flow with Fr in the range $Fr_* < Fr < Fr_c$, it would collapse through the radiation of long internal waves or columnar wave modes propagating ahead of the jump through the upstream flow, effectively 'blocking' and therefore modifying the upstream flow. (The width of the

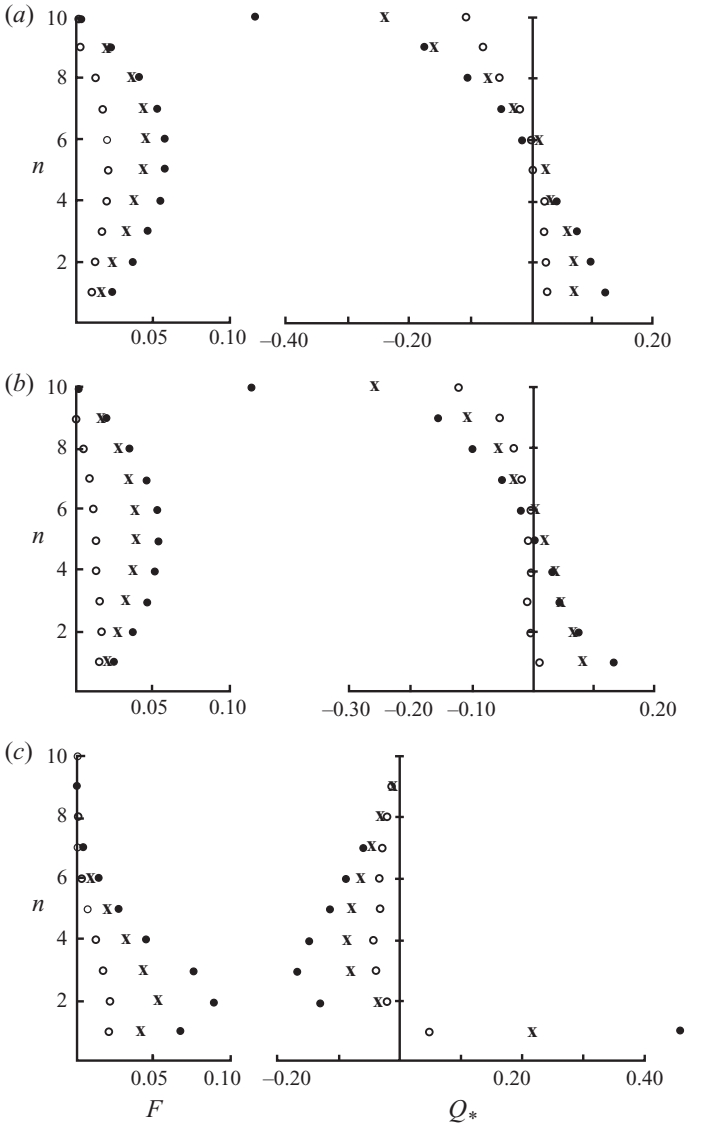

FIGURE 14. The non-dimensional upward diffusive and advective fluxes, F and Q_*, given by (B 7) and (B 3), respectively, for the cosine upstream flow equivalent to the η profile when $\eta = 0.4$. The fluxes are those across the 10 selected isopycnal surfaces (numbered from $n = 1$, the lowest, to $n = 10$ at $z = h_i$) which are marked in figure 3(c), as they pass through the transition region. (a) Case (i); (b) case (ii); (c) case (iv). (Case (iii) is not shown.) The fluxes are shown at: **o**, $Fr = 3$; **x**, $Fr = 5$; and ●, $Fr = 7$. The upward advective flux Q_* at the upper ($n = 10$) isopycnal is equal to $(1 - P)$. The uncertainty in the flux values is about 0.01.

front associated with a columnar mode propagating upstream will increase in time, t, roughly as $(Nt)^{1/3}$, where N is a measure of the buoyancy frequency; McEwan & Baines 1974; Baines 1995). Values of q, P, E and δ appear to change smoothly through the value $Fr = Fr_c$ (figures 7 and 10). A stable stationary hydraulic jump involves a multiplicity of modes that, together, combine to give a local change in isopycnal levels that can remain stationary in the flow, preserving the fluxes of volume, mass

and momentum passing through it and which will not decay through upstream wave radiation.

(iii) It follows that, in general, $Fr > Fr_*$ is a necessary condition for a stationary hydraulic jump to occur, as is also its equivalent, (26):

$$\int_0^H \left[u_1^2(z) - z^2 N_1^2(z)\right] \mathrm{d}z > 0,$$

where $N_1(z)$ is the buoyanscy frequency, but they may not be the most stringent. In the examples of the η profiles, where $Fr_* < Fr_c$, a more severe condition is that $Fr > Fr_c$. (This has not, however, been proved to hold for general upstream profiles of velocity and density, only for the η profiles.)

(iv) The minimum Ri in the η profile flows in which a stationary transition is possible are less than 1/4. This implies that the upstream flow may be dynamical unstable. The two-layer flow with $\eta = 1$ is known to be unstable, but $\eta = 0$ is stable. (Several other boundary flows are known in which the critical Ri is less than 1/4; Thorpe & Ozen 2007.) Although, for the η profile, it is necessary that the $\min(Ri_1) < 1/4$ for a hydraulic jump to occur, it is not, in general, necessary that a flow is dynamically unstable to Kelvin–Helmholtz instability. In cases where the upstream flow is dynamically unstable, transitions may result from a spatial Kelvin–Helmholtz instability, analogous to that studied by Koop & Browand (1979). The asymmetry of the downstream profiles when $\eta = 0.4$ (figure 9) and the values of $q_{1/2}$ (table 1 and §6.3) imply that mixing in the transitions is affected by the presence of the boundary. (The source of turbulence may affect the mixing in the transition region; see (xvi) below.).

The following conclusions apply for η profiles.

(v) When $Fr > Fr_*$, downstream flows are found that comply with the imposed conditions, but (except when conditions such as those in the four cases of maximum E, maximum P, minimum q and maximum E, but $P = 1$, are applied) these flows are not unique, i.e. with one upstream flow leading to just one single possible downstream flow. Although, for simplicity, examples have been selected in which the upstream density and velocity profiles are the same (i.e. $F_1 = f_1$ in (1) and (2)), profiles emerge downstream that are different from those upstream and in which the density differs from velocity: an assumption that the profiles of velocity and density are the same downstream as they are upstream is generally untenable. The cosine profiles lead to profiles and parameter values that are similar to those of the equivalent η profiles (figures 12–14 and figures 9–11, respectively): the discontinuities in the gradients of density and velocity in the latter upstream flows appear to have little effect on the downstream flows.

(vi) With $\eta = 0$ or 0.4, the size of the jumps in a flow with Froude number $Fr \geqslant Fr_c$ (the Froude number necessary for stationary jumps to be possible), are of finite amplitude. The smallest possible values of q are given by case (iii). As shown in figure 7(a), $q \sim 1.6$ at $Fr = Fr_c$, $= 8$ when $\eta = 0$, while from figure 10(a), $q \sim 1.45$ at $Fr = Fr_c$, $= 4.8$ when $\eta = 0.4$. The loss in non-dimensional energy flux, E, at $Fr = Fr_c$, is typically about 0.05 or more, depending on the selection of the extreme case in figures 7(c) and 10(c). Stable jumps have finite amplitudes and energy dissipation rates. It also follows that $q > 1$ (a rise in the thickness of the flowing layer, although not necessarily of all isopycnals) in a hydraulic jump, and q cannot be less than 1. Small-amplitude transitions with $q \sim 1$ occur when Fr is slightly greater than Fr_*. Since the Fr_* curve approaches the Fr_c curve as η tends to 1 in figure 4 it follows

that, although only finite amplitude jumps are possible for the two values chosen for η (0 and 0.4), small-amplitude jumps should be possible when η is near unity.

(vii) Some similarities can be seen in comparing the profiles of density and velocity in figures 6 and 9 for $\eta = 0$ and 0.4, respectively, e.g. in cases (i) and (ii) the density interfaces that appear in the downstream flows at $z/h_2 \approx 0.4$, and the relatively uniformity of velocity near $z = 0$. There are also many differences, e.g. in case (iii) the density at $\eta = 0.4$ more closely represents that of the upstream flow than do those for $\eta = 0$. It appears unlikely that there is some general form of the downstream flow profiles; the downstream flows depend not only on Fr but also on the shape of the upstream flow profiles, f_1 and F_1.

(viii) In the range of Fr considered, the amplitudes q of the jump (figures 7*a*, 10*a* and 13*a*), the loss E in dimensionless energy flux (figures 7*c*, 10*c* and 13*c*) and the dimensionless diapycnal fluxes F and $|Q_*|$ (figures 8, 11 and 14), all increase with Fr in each of the extreme cases. If the upstream values of ρ_0, Δ and h_1 are kept constant, whilst U_1 is varied, then since (8), $E = E'/(\rho_0 g \Delta h_1^2 U_1)$, the dimensional loss in energy flux, we can write $E' = (\rho_0 (g \Delta h_1)^{3/2} h_1) Fr^{1/2} E$, which increases even more rapidly with Fr than does E. The magnitude of the advective flux $|Q_A|$ and the diffusive flux F_A also increase with Fr more rapidly than do $|Q_*|$ and F, respectively. Values of $|Q_*|$ (figures 8, 11 and 14) are typically of order 0.1 in the range of Fr examined. The flux Q_* represents a cross-isopycnal entrainment rate divided by the vertically integrated upstream volume flux. If L is the width of the transition and w_e is the entrainment velocity (relating to (A 8) in Appendix A), $|Q_*| \sim w_e L/U_1 h_1$, equal to an entrainment coefficient, w_e/U_1, multiplied by the aspect ratio, L/h_1, of the transition. If the aspect ratio is of order unity, or greater, this implies an entrainment coefficient of order 0.1 (or less), in accord with commonly estimated values.

(ix) The maximum loss in energy flux (case (i)) occurs in conditions close to those in which entrainment is greatest (case (ii)); values of E when P is maximum are only slightly less than the values at maximum E (figures 7*c*, 10*c* and 13*c*).

(x) At values of Fr moderately greater than Fr_*, solutions for the downstream flows satisfying all the imposed conditions are found even when entrainment is excluded (case (iv), $P = 1$) but at higher values of Fr (e.g. when $Fr = 9$, $> Fr_c$ and with $\eta = 0$.), no downstream flows have been found with no entrainment: there must be entrainment into stable transitions at high Fr.

(xi) Downstream flows that are 'similar' to those upstream have corresponding values of E that are of magnitude comparable to those found in cases (i) and (ii) (figures 7*c*, 10*c* and 13*c*). The equivalent two-layer flows overestimate E when $\eta = 0$ (figure 7*c*) but give consistent values when $\eta = 0.4$. For such 'similar' upstream and downstream flows, however, there is no volume or mass flux across isopycnal surfaces within the transition region (§ 5). Lacking such diapycnal transports, transitions in such flows (or solutions incorporating an assumption of such similarity) cannot be regarded as being, in the usual sense, turbulent. Isopycnals simply bend and remain continuous within the rather passive transition region.

(xii) Even though the coefficients listed in table 2 indicate that in some cases convergence of the series (38) is (at best) slow, the forms of F_2 and f_2' found for the downstream flow are among the possible flows that satisfy the applied conditions ((*a*)–(*k*)). They may not, however, accurately represent the most extreme flows embodied in cases (i)–(iv), only those flows that can be represented by the four-term series (38); whilst the forms of the upstream flows can themselves be represented quite accurately by the series (Appendix G.1), not all possible functions that may describe the downstream flow are necessarily well represented. The results

are therefore indicative of the possible downstream flows, providing evidence that, in extreme cases, downstream flows exist that conform to the imposed conditions, rather than being definitive. The general consistency of the forms of F_2 and of f_2' as Fr increases and the relatively smooth trends in q, P and E versus Fr shown in figures 7, 10 and 13 indicate a fairly regular pattern of behaviour even though the representation of the downstream flow by (38) is approximate and limited. The maximum energy flux lost from a given upstream flow is a function of Fr (or q) and provides useful information about the greatest dissipation of energy that can occur in the deep ocean flows and of its effect on ocean mixing (Thorpe 2007).

(xii) Although not demonstrated in the above analysis, it may be expected that, as in single-layer hydraulic jumps, waves in the downstream flow can travel in both the upstream and downstream directions. This has not been tested in every case, but in those where the downstream flow can be approximately represented by an η profile (e.g. in case (iv) at $\eta = 0$ when $Fr = 7$, and case (iii) when $\eta = 0.4$ and $Fr = 3$ and 7), the Froude number of the downstream flow is well below the value Fr_c at which upstream-travelling waves are prevented. If the downstream flows have properties similar to those of the η profiles, $\min(Ri_2) > 1/4$ (condition (h)) may be sufficient to ensure waves can travel in both directions as predicted by Bell (1974). Since $S \leqslant 1$ (condition (i)) the Froude numbers of the downstream flows are less than, or equal to, their corresponding critical values, Fr_*. If also, for these flows, the corresponding $Fr_* \leqslant Fr_c$, it again follows that they will support both upstream- and downstream-travelling waves.

(xiv) No account has been taken, however, of the possible downstream flux of energy from a transition region through the internal waves. When Fr_* is only slightly greater than Fr_c (i.e. when $\eta \sim 1$, figure 4), jumps with Fr marginally greater than Fr_c (and therefore not much greater than Fr_*) are likely to occur in which internal waves transport energy from the transition, much as waves in single-layer undular bores are known to do, or as do waves in circular two-layer jumps at relatively low Froude numbers (Thorpe & Kavčič 2008; see also case (vi)).

(xv) There is no formal reason for selecting one or other (or any) of the four extreme cases chosen in § 6.1, or for supposing that any one of them is appropriate, and there remains the question, 'What additional conditions may, in practise, constrain the downstream flow so that only one can correspond to a given upstream flow?' – supposing that the downstream flow is uniquely determined by the upstream. A more rigorous examination of the stability of the downstream flow than is afforded by the condition (h) ($\mathrm{Min}(Ri_2) \geqslant 1/4$) or condition ($i$) – see footnote to Appendix A – might lead to a more severe constraint on the possible downstream flows. A reviewer kindly suggests that angular momentum conservation may provide a further limit (see Hornung, Willert & Turner 1995) but it is not clear how this may be applied to a stratified, possibly turbulent, transition.

(xvi) In a real situation (e.g. in the ocean) it is likely that conditions far downstream of a transition, a region in which upstream wave propagation can occur, control the downstream flow structure and consequently the nature of a transition. It is also possible that, in real flows, boundary slope and friction on the boundary (Swaters 2009), and the upward radiation of internal waves in stratified overlying water have significant effects, modifying the conservation of momentum flux. (The flux of momentum associated with radiating waves may amount to a few percent of that carried by the flow (see e.g. Pham, Sarkar & Brucker 2009). Introduction of stratification in the upper layer, however, introduces complications related to the

density of fluid entrained by a jump and the pressure within the moving layer, that make analysis more difficult.)

(xvii) It is possible that the turbulent processes within the transition region are not adequately represented by the flux conditions, (j) and (k). This concern relates to the uncertain assessment of the diapycnal flux and dissipation within the transition (as expressed, e.g. by the note below (16)). The selection of $\Gamma = 0.2$ is somewhat *ad hoc*, and Γ may vary (Peltier & Caulfield 2003), perhaps with the flow Reynolds and/or Richardson numbers. If, for example, the transition is like a spilling or plunging surface wave breaker, with a jump representing a mixing layer (as suggested by Peregrine & Svendsen 1978, and supported with illustrations by Hoyt & Sellin 1989), or with single or multiple unsteady rotors (or 'rollers') producing static instability and initiating turbulence in the downstream flow (Yeh 1991; Svendsen *et al.* 2000), or if a near-bed rotor/bolus develops, as in large-amplitude internal waves, will the flux assumptions hold true and will the entrainment parameter w_e/U_1 (on which the relative magnitude of the KE of the entrained flow depends; Appendix A) still be small? Information is required about the nature of the turbulent flow within a transition and how it should be represented or 'parametrized'.

7.2. *Application*

Although some measurements upstream and downstream of the suspected location of jumps in the abyssal ocean have been obtained (e.g. Polzin *et al.* 1996), there are presently too few observations to establish the certain existence there of hydraulic jumps. More studies are planned (A. Thurnherr and J. Mackinnon, private communication 2009). In principle, profiles of the mean flow measured upstream and downstream of a suspected jump could, if $Fr > Fr_*$, be used to estimate the loss in energy flux (8) and the diapycnal fluxes (B 3) and (B 7) within the transition region.

A 'pseudo Froude number', $\langle U\rangle/\langle N\rangle H$, with a critical value assumed to be about unity, has been used as a guide to test whether flows observed in abyssal valleys in the deep ocean are likely to be subcritical or supercritical (St Laurent & Thurnherr 2007; MacKinnon *et al.* 2008), where $\langle U\rangle$ and $\langle N\rangle$ are the depth-averaged velocity and buoyancy frequency over the moving layer of depth H. This Froude number can be compared with that derived for the η profiles, with the implicit assumption that the effects of stratification and flow above the moving layer can be ignored. Calculating $\langle U\rangle$ and $\langle N\rangle$ for the η profile (27), and putting $H = h_1$:

$$(\langle U\rangle/\langle N\rangle H)^2 = Fr(1+\eta)^2/[8(1-\eta)] \tag{39}$$

with $Fr = U_1^2/(g\Delta H)$. Values of $\langle U\rangle/\langle N\rangle H$ derived from (39), with $Fr = Fr_*$ and $Fr = Fr_c$, are shown as functions of η in figure 15.

The flow through the Lucky Strike segment of the Mid-Atlantic Ridge studied by St Laurent & Thurnherr (2007) may approximately be represented by the η profile (27) with values of η in the range 0–0.4. The reported values of $\langle U\rangle/\langle N\rangle H$ are 0.92 upstream and (0.36–0.37) downstream of the location of a possible hydraulic jump. Although the downstream values lie below both Fr_* and Fr_c in figure 15, consistent with a subcritical flow, the upstream value is between Fr_* and Fr_c where the continuity equations for a jump are satisfied, but where upstream-going waves may be possible, relaxing any transition that occurs.

Flows in the ocean are unsteady, often tidally modulated. Jumps may be inherently transient, depending on the strength of the tidal component (e.g. Farmer & Armi 1999), with Fr perhaps varying from $> Fr_c$ to $< Fr_*$. The time required for disintegration of a jump may be considerable if Fr is near Fr_* since, as shown in

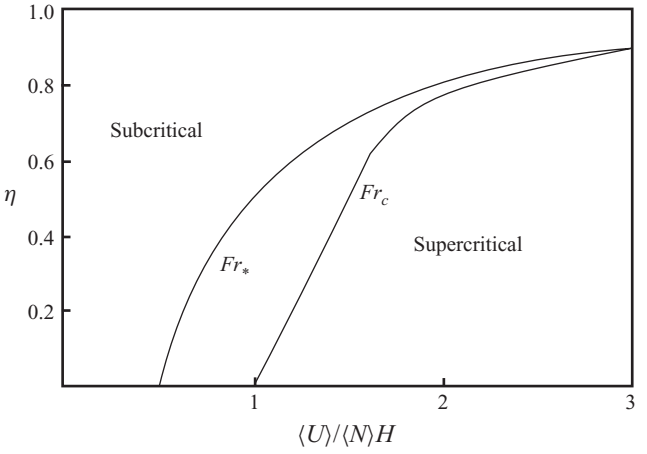

FIGURE 15. The critical values of $\langle U\rangle/\langle N\rangle H$ as functions of η, corresponding to those labelled Fr_* and Fr_c in figure 4 and calculated using (39).

figure 4, the speed of long internal waves is then small: the curve $(-c/U) = 10^{-1}$ corresponds roughly to $Fr = Fr_*$ when $0 \leqslant \eta \leqslant 0.4$ with smaller speeds in $Fr_* < Fr < Fr_c$. With flows in the abyssal ocean typically of the order of 0.2 m s^{-1}, the distance that waves could propagate over an M_2 tidal period from a hydraulic jump in which Fr had fallen from Fr_c to Fr_* would, over a tidal period, be about 1 km, a relatively small distance. In addition to direct investigations to establish the existence of hydraulic jumps, further measurement is required of the flows through abyssal valleys. Calculations should be made of the propagation characteristics of the internal waves that flows can support.

7.3. *Summary*

Stationary hydraulic jumps occur in some stratified boundary shear flows. Stable jumps may form when Fr exceeds a value Fr_c at which mode 1 long internal waves or columnar modes cannot propagate upstream, and where $\min(Ri_1) \leqslant 1/4$. In the η profile flows and in other flows considered in Appendix H, the critical Froude number Fr_c exceeds Fr_*, the least value at which the equations of conservation of volume, mass and momentum flux are satisfied. For $Fr < Fr_*$, stationary jumps cannot occur; for $Fr_* < Fr < Fr_c$, jumps may occur but will not be sustained; for $Fr > Fr_c$, jumps of finite amplitude (q greater than about 1.4) are possible, generally accompanied by entrainment from the overlying fluid but with an upstream flow that may be dynamically unstable, an exception being when $\eta = 0$; it is not, in general, necessary that a flow is dynamically unstable to Kelvin–Helmholtz instability for a jump to occur.

I am grateful to Mrs Kate Davis for assistance in preparing the figures and to Professor Alan Davies for use of a computer.

Appendix A. Conservation equations in general form

With velocity given by (1) and density by (2), conservation of volume flux per unit width from upstream ($i = 1$) to downstream ($i = 2$) through the assumed transition is

satisfied by

$$U_1 h_1 \int_0^1 F_1(x)\,\mathrm{d}x + Q = U_2 h_2 \int_0^1 F_2(x)\,\mathrm{d}x, \tag{A 1}$$

where Q is the flux of fluid of density $\rho_0(1-\Delta)$, per unit channel width, entrained from the overlying uniform layer into the moving lower-layer flow. Defining an entrainment factor P as

$$P = Q \Big/ \left(U_1 h_1 \int_0^1 F_1(x)\,\mathrm{d}x \right) + 1, \tag{A 2}$$

(A 1) gives

$$P = U_2 h_2 \int_0^1 F_2(x)\,\mathrm{d}x \Big/ \left(U_1 h_1 \int_0^1 F_1(x)\,\mathrm{d}x \right), \tag{A 3}$$

which is >1 if $Q>0$ (i.e. there is positive entrainment into the transition region).

The conservation of mass flux per unit width, including the flux $Q\rho_0(1-\Delta)$ from the overlying layer, leads in general, using (A 1), to a further relation:

$$U_1 h_1 \int_0^1 f_1(x)F_1(x)\,\mathrm{d}x = U_2 h_2 \int_0^1 f_2(x)F_2(x)\,\mathrm{d}x, \tag{A 4}$$

so that (A 3) can be written as

$$P = \int_0^1 f_1(x)F_1(x)\,\mathrm{d}x \int_0^1 F_2(x)\,\mathrm{d}x \Big/ \left(\int_0^1 f_2(x)F_2(x)\,\mathrm{d}x \int_0^1 F_1(x)\,\mathrm{d}x \right). \tag{A 5}$$

Taking a volume with vertical surfaces in the steady flows upstream and downstream of a transition, a lower surface in the plane, $z=0$, where friction is neglected, and an upper surface in the zero-stress region above the flowing layer, momentum conservation (conservation of $\int p_i\,\mathrm{d}z + \int(\rho_i u_i)u_i\,\mathrm{d}z$, where p_i is the pressure, assumed to be hydrostatic upstream and downstream of a transition) leads to

$$U_1^2/g\Delta h_1 = 2q\left[q^2\int_0^1 xf_2(x)\,\mathrm{d}x - \int_0^1 xf_1(x)\,\mathrm{d}x\right] \Big/ \left[\int_0^1 F_1^2(x)\,\mathrm{d}x \left\{ q - P^2 \times \int_0^1 F_2^2(x)\,\mathrm{d}x \left(\int_0^1 F_1(x)\,\mathrm{d}x \right)^2 \Big/ \left[\int_0^1 F_1^2(x)\,\mathrm{d}x \left(\int_0^1 F_2(x)\,\mathrm{d}x \right)^2 \right] \right\} \right] \tag{A 6}$$

as a condition for a transition to occur, where we have used the equality

$$\int_0^1 \int_x^1 f(y)\,\mathrm{d}y\,\mathrm{d}x = \int_0^1 xf(x)\,\mathrm{d}x.$$

The loss in energy flux per unit width, E' (the change in the sum of the KE flux, $\int(\rho_i u_i^2/2)u_i\mathrm{d}z$, and the potential energy flux, $\int g\rho_i z u_i\mathrm{d}z$, accounting for the work done by the pressure force, $\int p_i u_i\mathrm{d}z$) is given by Thorpe & Ozen (2009). Writing $Fr = U_1^2/g\Delta h_1$, it can be expressed in non-dimensional form as

$$E \equiv E'/\left[\rho_0 g \Delta h_1^2 U_1\right] = (Fr_1/2)\left\{ \int_0^1 F_1^3(x)\,\mathrm{d}x - \int_0^1 F_2^3(x)\,\mathrm{d}x \left[\int_0^1 F_1(x)\,\mathrm{d}x \Big/ \int_0^1 F_2(x)\,\mathrm{d}x \right]^3 P^3/q^2 \right\}$$

$$+2\left\{\int_0^1 xf_1(x)F_1(x)\,\mathrm{d}x+\int_0^1 F_1(x)\int_x^1 f_1(y)\,\mathrm{d}y\,\mathrm{d}x\right\}-2q\left\{\int_0^1 f_1(x)F_1(x)\,\mathrm{d}x\Big/\right.$$
$$\left.\times\int_0^1 f_2'(x)F_2(x)\,\mathrm{d}x\right\}\left\{\int_0^1 xf_2'(x)F_2(x)\,\mathrm{d}x+\int_0^1 F_2(x)\int_x^1 f_2'(y)\,\mathrm{d}y\,\mathrm{d}x\right\},\qquad(\mathrm{A}\,7)$$

provided that the KE flux carried by the entrained flow Q is negligible, with $Fr=U_1^2/g\Delta h_1$ given by (A 6). With no source of energy flux within the transition, E' cannot be negative if the transition is to be physically possible.

The KE flux of the entrained flow with a mean entrainment velocity, $w_e=Q/L$, where L is the length of the transition (figure 1), divided by the change in the KE flux of the horizontal flow, is equal to $\mu(w_e/U_1)^2$, where

$$\mu=(P-1)\int_0^1 F_1\,\mathrm{d}x\Big/\left[\int_0^1 F_1^3\,\mathrm{d}x-(P^3/q^2)\int_0^1 F_2^3\mathrm{d}x\left(\int_0^1 F_1\,\mathrm{d}x\Big/\int_0^1 F_2\,\mathrm{d}x\right)^3\right].\qquad(\mathrm{A}\,8)$$

Although μ increases with Fr, it is less than unity in all the cases examined here, and since the entrainment parameter, w_e/U_1, is generally less than 0.1 (Turner 1973), the KE flux carried by the entrained flow Q is relatively small and is neglected.

The condition that the downstream flow cannot undergo a further transition is that its Froude number is subcritical, or from (22):

$$U_2^2/(gf_2(0)\Delta h_2)\leqslant 4\int_0^1 xf_2(x)\,\mathrm{d}x\Big/\int_0^1 F_2^2(x)\,\mathrm{d}x.\qquad(\mathrm{A}\,9)$$

Using (A 4), this can be expressed in terms of a stability parameter S:

$$S\equiv Fr\Big/\left\{4q^3\left[\int_0^1 xf_2(x)\,\mathrm{d}x\Big/\int_0^1 F_2^2(x)\,\mathrm{d}x\right]\left[\int_0^1 f_2(x)F_2(x)\,\mathrm{d}x\Big/\int_0^1 f_1(x)F_1(x)\,\mathrm{d}x\right]^2 f_2(0)\right\},\qquad(\mathrm{A}\,10)$$

where $S\leqslant 1$ implies stability and $S>1$ implies that the downstream flow can undergo a further shape-preserving transition, a condition of instability. (This condition may be more severe than is necessary. As shown in § 4.3, for some flows Fr_* is not the critical Fr, and terms on the right-hand side of (A 9) and (A 10), derived from Fr_* defined in (22), should be greater. Moreover, a reviewer has kindly pointed out that the condition is not essential because supercritical flows may be possible both upstream and downstream of jumps (Baines 1995, ch. 3).)

Appendix B. Expressions for the diapycnal fluxes within the transition

With reference to figure 1, the net volume flux into ABCD must be zero since the fluid is incompressible and, since there is no flux through CD, the vertical volume flux per unit width through AB is

$$Q_A=\int_0^{z1}u_1(z)\,\mathrm{d}z-\int_0^{z2}u_2(z)\,\mathrm{d}z.\qquad(\mathrm{B}\,1)$$

Using (1) it follows that

$$Q_A=U_1h_1\int_0^{x1}F_1\,\mathrm{d}x-U_2h_2\int_0^{x2}F_2\,\mathrm{d}x,\qquad(\mathrm{B}\,2)$$

where $x1 = z1/h_1$, $x2 = z2/h_2$. (Equation (A 1) follows if $x1 = x2 = 1$, recalling that at the top of the transition region, $Q_A = -Q$.) Using (A 3) to eliminate U_2h_2:

$$Q_* \equiv Q_A \Big/ \left(U_1 h_1 \int_0^1 F_1 \,\mathrm{d}x \right)$$
$$= \left[\int_0^1 F_2 \,\mathrm{d}x \int_0^{x1} F_1 \,\mathrm{d}x - P \int_0^1 F_1 \,\mathrm{d}x \int_0^{x2} F_2 \,\mathrm{d}x \right] \Big/ \left[\int_0^1 F_1 \,\mathrm{d}x \int_0^1 F_2 \,\mathrm{d}x \right] \quad \text{(B 3)}$$

which reduces to (3) if $x1 = x2 = 1$.

We next consider the mass flux per unit width into the region ABCD. This is comprised of the advective and diffusive fluxes of mass or density:

$$\int_0^{z1} \rho_1 u_1(z) \,\mathrm{d}z - \rho_A Q_A - F_A = \int_0^{z2} \rho_2 u_2(z) \,\mathrm{d}z, \quad \text{(B 4)}$$

where F_A is the diffusive flux of density through AB (there is again no flux through CD, and AD and BC are taken sufficiently far upstream and downstream to ensure there is no horizontal diffusive flux through these surfaces). Using (1) and (2), and substituting for Q_A from (B 2), (B 4) can be written as

$$F_A = 2\Delta\rho_0 \left[U_1 h_1 \left(\int_0^{x1} f_1 F_1 \,\mathrm{d}x - f_A \int_0^{x1} F_1 \,\mathrm{d}x \right) - U_2 h_2 \left(\delta \int_0^{x2} f_2' F_2 \,\mathrm{d}x - f_A \int_0^{x2} F_2 \,\mathrm{d}x \right) \right], \quad \text{(B 5)}$$

where $f_A = f_1(x1) = f_2(x2)$ (equality because A and B are on the same isopycnal surface). Using (A 4),

$$U_2 h_2 = U_1 h_1 \int_0^1 f_1 F_1 \,\mathrm{d}x \Big/ \left(\delta \int_0^1 f_2' F_2 \,\mathrm{d}x \right), \quad \text{(B 6)}$$

and eliminating δ using (4) gives

$$F \equiv F_A/(\Delta\rho_0 U_1 h_1) = 2 \Bigg\{ \int_0^1 F_2 \,\mathrm{d}x \int_0^1 f_2' F_2 \,\mathrm{d}x \left[\int_0^{x1} f_1 F_1 \,\mathrm{d}x - f_A \int_0^{x1} F_1 \,\mathrm{d}x \right]$$
$$- \int_0^1 F_2 \,\mathrm{d}x \int_0^1 f_1 F_1 \,\mathrm{d}x \int_0^{x2} f_2' F_2 \,\mathrm{d}x + P f_A \int_0^{x2} F_2 \,\mathrm{d}x \int_0^1 F_1 \,\mathrm{d}x \int_0^1 f_2' F_2 \,\mathrm{d}x \Bigg\}$$
$$\Big/ \left[\int_0^1 F_2 \,\mathrm{d}x \int_0^1 f_2' F_2 \,\mathrm{d}x \right]. \quad \text{(B 7)}$$

Putting $x1 = x2 = 1$ and $f_A = 0$, this is consistent with there being no diffusive flux of density through the zero vertical density gradient of the fluid above the upper surface of the transition.

Appendix C. Maximum and minimum loss in energy flux

The entrainment factor P appears only in the first term of (8) and, all the integral terms in the equation being positive, the term in P is negative. If the upstream flow (F_1, f_1 and Fr) is given then, for specified functions (F_2 and f_2') determining the downstream flow, the maximum value of E given by (8) at any value of the jump amplitude q is found when the entrainment factor P is a minimum but consistent with (7) for Fr. The term in (8) within the $\{\ldots\}$ brackets represents the rate of loss of KE flux in the transition, and (for a specified upstream flux) this is greatest when the

downstream flux is least. (It may be foreseen that the downstream flux is likely to be least when P is least: from (A 1), the downstream volume flux is least when the flux of entrained water, Q, is a minimum.)

Differentiating (8) with respect to q at a given P, E is a maximum when

$$q = P\left\{\left(Fr\int_0^1 F_2^3\,\mathrm{d}x\right)\int_0^1 f_2'F_2\,\mathrm{d}x\Big/\left[\int_0^1 f_1F_1\,\mathrm{d}x\left(\int_0^1 xf_2'F_2\,\mathrm{d}x + \int_0^1 F_2\int_x^1 f_2'(y)\,\mathrm{d}y\,\mathrm{d}x\right)\right\}^{1/3}\left(\int_0^1 F_1\,\mathrm{d}x\Big/\int_0^1 F_2\,\mathrm{d}x\right)\right], \quad (C\,1)$$

provided that this value can be reached when (7) is satisfied. If the downstream profiles, F_2 and f_2', remain unchanged (which is not necessarily the case), the value of q at which E is a maximum increases as $Fr^{1/3}$.

These results apply, however, only if the downstream flow given by F_2 and f_2', is specified and independent of Fr, q and P, which (as is evident in § 6) is not true in general but is, for example, for the similar downstream flows described in § 5.

Appendix D. The smallest Fr

Putting $F_2 = F_1$, $f_2' = f_1$ and $P_0 = 1$ in (7) we obtain

$$Fr = 2\left[\int_0^1 xf_1(x)\,\mathrm{d}x\Big/\int_0^1 F_1^2(x)\,\mathrm{d}x\right]\Theta, \quad (D\,1)$$

where $\Theta = \{q(q^2 - P)/[P(q - P^2)]\}$ and $P \geqslant 1$. The variation of Θ with q and P is shown in figure 16(a). The value of Θ tends to zero at $q = 0$ and $P^{1/2}$, and to infinity at $q = P^2$. The minimum of Θ with respect to q, found by differentiation, is where $2q^3 - 3q^2P^2 + P^3 = 0$, and putting $P = 1 + \varepsilon$ where $0 \leqslant \varepsilon \ll 1$, and neglecting terms of higher order, we find $q \approx 1 \pm \varepsilon^{1/2}$, and $\Theta \approx 2(1 \pm \varepsilon^{1/2})$, the positive signs corresponding to the minimum value of Θ. The limiting value, $\Theta = 2$, is smoothly approached as q tends to 1 (a jump of zero amplitude) and P tends to 1, implying no entrainment, as shown in figure 16(b). The limiting value of Fr is therefore as given in (22).

From (A 7), the loss in energy flux when $F_2 = F_1$, $f_2' = f_1$ is

$$E = (Fr_1/2)\left\{\int_0^1 F_1^3(x)\,\mathrm{d}x(1 - P^3/q^2)\right\} + 2(1-q)\left\{\int_0^1 xf_1(x)F_1(x)\,\mathrm{d}x + \int_0^1 F_1(x)\int_x^1 f_1(y)\,\mathrm{d}y\,\mathrm{d}x\right\}, \quad (D\,2)$$

and this tends to zero as P and q tend to unity and is negative when $1 < q < P^{1/2}$ where, as shown in figure 16(a), $\Theta > 0$. Although it is shown in Appendix F that $E < 0$ if $q < 1$ for the η profiles, it is not evident that $E < 0$ when $q < 1$ for all possible profiles, and jumps to a smaller flow thickness, with $q < 1$, might be possible.

Appendix E. Long waves in an η profile

Analytical solutions can be found for the speed of long internal waves in flows with η profiles. When the Boussinesq approximation is valid, the Taylor–Goldstein equation for neutral internal waves in the region $\eta h \leqslant z \leqslant h$ where the shear and N are constant is

$$\mathrm{d}^2\varphi/\mathrm{d}z^2 + \{N^2/(u-c)^2 - k^2\}\varphi = 0 \quad (E\,1)$$

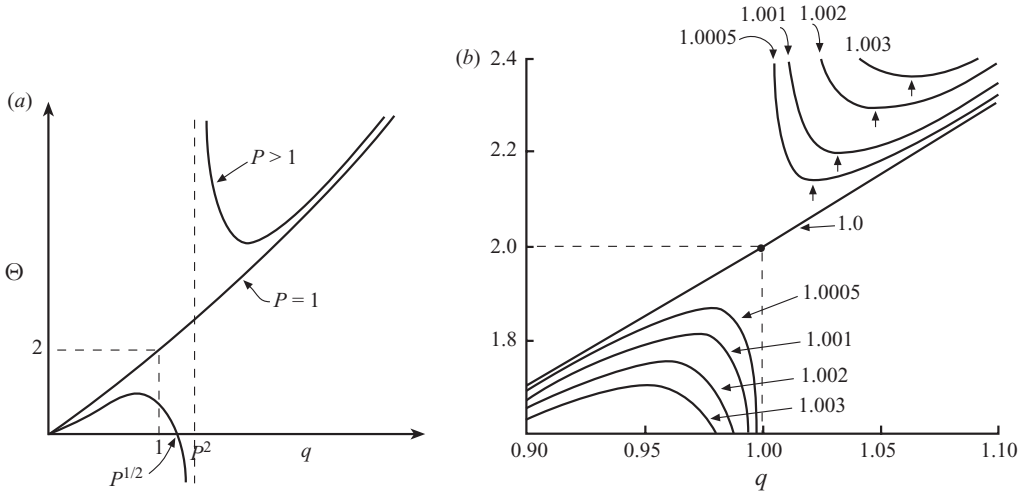

FIGURE 16. The variation of Θ with q and P. (a) Θ as a function of q when $P=1$ and at a value of $P>1$. (b) Details of the variation of Θ near $q=1$ for (labelled) values of P, also near 1. Arrows mark the minimum values of Θ, tending towards $\Theta=2$ at $q=1$, $P=1$.

with appropriate boundary conditions, where the stream function is $\psi(x,z,t)=\phi(z)\exp[ik(x-ct)]$, and k is the real wavenumber in the horizontal x direction of a flow, $u(z)$, in which the buoyancy frequency is N. When $u=U_1(h-z)/[h(1-\eta)]$ as in (27), and in the long-wave limit, $kh=0$, this reduces to

$$[(U_1(h-z)-ch(1-\eta)]^2\mathrm{d}^2\varphi/\,\mathrm{d}z^2+N^2(1-\eta)^2\varphi=0 \tag{E 2}$$

with the solution

$$\varphi=A_1\{[(U_1(h-z)-ch(1-\eta)]/[Nh^2(1-\eta)]\}^{p^1} + A_2\{[(U_1(h-z)-ch(1-\eta)]/[Nh^2(1-\eta)]\}^{p^2}, \tag{E 3}$$

where

$$p^n=\{1\pm\sqrt{[1-(2Nh(1-\eta)/U_1)^2]}\}/2=(1\pm r)/2,\ n=1,2, \tag{E 4}$$

with

$$r=\sqrt{[1-(2Nh(1-\eta)/U_1)^2]}. \tag{E 5}$$

Boundary conditions are found by matching the vertical velocity and pressure at $z=\eta h+a\exp[ik(x-ct)]$ and $z=h+b\exp[ik(x-ct)]$, where a and b are the amplitudes of small displacements, to those of irrotational potential flow solutions in $0\leqslant z\leqslant\eta h$ and $z\geqslant h$, in the usual way, or by taking $\varphi=0$ at $z=0$ if $\eta=0$.

When r is real, putting the η profile value, $N^2=2\Delta g/(h(1-\eta))$ and $U=U_1$, (E 5) gives

$$Fr=U_1^2/g\Delta h_1=8(1-\eta)/(1-r^2)>8(1-\eta). \tag{E 6}$$

From (28), $8(1-\eta)$ is the value of Fr when $\min(Ri)=1/4$, a curve shown in figure 4. The boundary conditions lead to a dispersion relation:

$$[(-c/(U_1-c)]^r=[(1+r)/(1-r)]\{3\eta-2-r\eta+2(1-\eta)(c/U_1)\}/ \times\{3\eta-2+r\eta+2(1-\eta)(c/U_1)\}. \tag{E 7}$$

Real roots for c/U_1 are possible only if $c/U_1>1$ or $c/U_1<0$, i.e. when there is no critical layer where the speed of the mean flow matches the speed c. Roots can be

found as $c/U_1 \to 0-$ (the limit for upstream travelling waves) only if $\eta > 2/3$; there are no wave solutions when $\eta < 2/3$ if $Fr > 8(1-\eta)$.

If, however, r is imaginary, $= \mathrm{i}R$, say,

$$Fr = U_1^2/g\Delta h_1 = 8(1-\eta)/(1+R^2)) < 8(1-\eta), \tag{E 8}$$

and the dispersion relation becomes

$$(R/2)\ln[(U_1-c)/(-c)] = \tan^{-1}(-R/\Psi), \tag{E 9}$$

where

$$\Psi = 1 - \eta(1+R^2)/[2(1-\eta)(1-c/U_1)]. \tag{E 10}$$

Solutions ($R \to 0+$) with $c/U \to 0-$ are found provided $\eta < 2/3$ and $Fr < 8(1-\eta)$. Differentiating (E 9) with respect to h, we find that $\partial c/\partial h < 0$ as $c/U_1 \to 0-$, whilst $\partial c/\partial h > 0$ if $c/U_1 \to 1+$, properties that are in accord with those leading to a convergence of characteristics and the formation of hydraulic jumps in single-layer flows (e.g. Lighthill 1978).

Values of $Fr = Fr_c$ where $-c/U_1 = 0$ are shown in figure 4 in the range $0 \leqslant \eta \leqslant 1$. Also shown are the phase speeds (equal to the group speeds) of the long and relatively fast (mode 1) waves when $Fr < Fr_c$ calculated by numerical solution of (E 7) and (E 9). The existence of upstream propagating waves when $\min(Ri) = 1/4$ (e.g. when $Fr < Fr_c$ in $\eta < 2/3$) is consistent with Bell's theorem (Bell 1974). In a two-layer flow where $\eta = 1$, although the flow is always unstable through Kelvin–Helmholtz instability to sufficiently short waves, analytical solutions can be found for long waves: $c/U_1 = 1 \pm (2/Fr)^{1/2}$ (e.g. Thorpe & Kavčič 2008). Waves can travel upstream if $Fr < 2$ with speeds $-c/U_1 = (2/Fr)^{1/2} - 1$, and, for example, $-c/U_1 = 0.1$ when $Fr = 1.65$, and $-c/U_1 = 0.01$ when $Fr = 1.96$, as shown in figure 4. No waves propagate upstream when $\eta = 1$ if $Fr > 2$.

Appendix F. Formulae for E in shape preserving flows

If the η-profile, (27), is chosen for the upstream flow, (35) gives

$$E = Fr(1+3\eta)(1-P^3/q^2)/8 - (q-1)[2(1+2\eta+3\eta^2)+3(1+\eta)^2]/12, \tag{F 1}$$

from which it can be shown that E is positive for all $q > 1$ but negative if $q < 1$. The corresponding shape preserving cosine profile (30) leads to

$$E = Fr[16-3\pi+\eta(16+3\pi)](1-P^3/q^2)/64 - (q-1) \times [8(1+\eta)^2 - \pi(1-\eta^2) + (\pi^2-8)(1-\eta)^2]/16, \tag{F 2}$$

and again $E > 0$ if $q > 1$ and < 0 if $q < 1$.

Appendix G. The method of solution and the sine series (38)

G.1. *Procedure for numerical solution*

The upstream flow and value of Fr are selected. There are eight unknowns, a_m and b_m, $m = 1$–4, involved in using (38), and each is ascribed a range of seven possible values, beginning with relatively wide ranges. These values of a_m and b_m are used to find profiles of F_2 and f_2'. The profiles of F_2 and f_2' that satisfy conditions (a) and (c) are then used to determine the integral terms in (A 1)–(A 10). The Froude number Fr is calculated using (7) for typically 50 values of q and some 20 values of P (q

increasing from q_m (18) and P decreasing from P_m (19)), leading to a total of about 10^9 estimates of Fr. Those that give $Fr \leqslant 0$ (condition (g)) and are more than ± 0.01 from the selected value of Fr are discarded: depending on η and Fr, typically about 5×10^6 values lie within the range. Calculations are then made of $\min(Ri_2)$ using (9), S (10) and E (8), with possible values discarded according the conditions (h), (i) and (f), respectively, leaving typically about 10^6 'possible' values. Values of Γ are calculated using (17). Negative diffusive flux values are discarded in accordance with condition (j), leaving some 5×10^5 values, before condition (k) is applied, retaining only some 10^4 (or fewer – especially in case (iii)) values of Γ that are between 0.19 and 0.21.

Of the remaining sets of values of a_m and b_m, those that lead to optimal values of q, E or P as selected to comply with cases (i)–(iv) in § 6.1 form possible 'solutions' for downstream flows that pass the several imposed conditions. If any of these values of a_m or b_m are at the bounds of their chosen range, the ranges are revised and extended accordingly and, once the ranges span the possible solutions, their width is decreased to refine the selections and to obtain more precise estimates of a_m and b_m. It typically requires four to six reiterations until solution values of a_m and b_m are found to within factors of 0.01.

G.2. *Fit of the series (38) to the selected upstream profiles*

The representation (38), but with an unbounded sine series (m extending to infinity), is equal to the η-profile, (27), when $a_m = 2\sin(m\pi\eta)/[(m\pi)^2(1-\eta)]$.

The fit is exact if $\eta = 0$, with $a_m = 0$. If $\eta = 0.4$ we find $a_1 = 0.321$, $a_2 = 0.0496$, $a_3 = -0.0221$ and $a_4 = 0.0201$. (The following term is $a_5 = 0$.) The root mean square difference between the truncated four-term series (38) and the η-profile is then 0.00838, indicating that (38) gives a reasonably close fit. The maximum difference between the series expression and (27) is 0.033 at $x = 0.4$, the point where the gradient of the η-profile is discontinuous. (If $\eta = 0.7$, then $a_1 = 0.546$, $a_2 = -0.161$, $a_3 = 0.0232$ and $a_4 = 0.0248$. The root mean square difference between the series (38) and the η-profile is 0.0233: (38) giving a reasonably close fit. The maximum difference between the two series is 0.054 at $x = 0.72$. In the two-layer flow when $\eta = 1.0$, the constants $a_m = 2/(m\pi)$, and have relatively slow convergence with increasing m, and for this reason calculations have been limited to $\eta \leqslant 0.7$.)

The series (38) can similarly be fitted to the cosine profile (30) scaled to the η-profile with $a_m = A/[\pi m(m^2 - A)][\cos(m\pi B) + (-1)^m]/[(m\pi)^2(1-\eta)]$, where $A = \{[2(1+\eta) + \pi(1-\eta)]/[2\pi(1-\eta)]\}^2$ and $B = [2(1+\eta) - \pi(1-\eta)]/[[2(1+\eta) + \pi(1-\eta)]$, giving $a_1 = 0.165$, $a_2 = 0.134$, $a_3 = -0.0279$ and $a_4 = 0.00193$ when $\eta = 0.4$. The root mean square difference between the series (38) and the cosine-profile (30) is 0.00619, again indicating a reasonably close fit. The maximum difference between the two series is less than 0.012.

It is acknowledged, however, that the best fit of the series (38a) leads, in $0 \leqslant x \leqslant \eta_1$ of (27) and $0 \leqslant x \leqslant l/h_1'$ of (30), to regions where $\mathrm{d}f_2'(x)/\mathrm{d}x > 0$, the sine series failing to represent the constant density exactly. At some levels the density variable f_2' exceeds unity, its value at $z = 0$. For a downstream flow having an η-profile with $\eta = 0$, the problem does not arise but, if $\eta > 0$, the values a_i in the sine series representations of downstream flows with η- or cosine-profiles have to be modified if the series is to satisfy the conditions (c) and (d) of § 2.

Appendix H. Other upstream profiles

The values of Fr_c, Fr_* and c shown in figure 4 depend on the profiles, the η profiles, selected to represent the upstream flow. If, for example, the density profile remains unchanged with f_1 given by (27) but a uniform shear is introduced in the lower layer reducing the flow to zero at $z=0$:

$$F_1 = \begin{cases} x/\eta, & \text{if } 0 \leqslant x \leqslant \eta \leqslant 1, \\ (1-x)/(1-\eta), & \text{if } \eta \leqslant x \leqslant 1, \end{cases} \tag{H 1}$$

then (22) gives

$$Fr_* = 2(1+\eta+\eta^2), \tag{H 2}$$

instead of (29). The speed of long waves can be found as in Appendix E. There are upstream travelling waves ($-c/U>0$) for all Fr except for $\eta=0$, when the flow reduces to the η profile with $\eta=0$ and the phase speeds are as shown at $\eta=0$ in figure 4, being zero if $Fr \geqslant 8$. When $\eta=1$, upstream travelling solutions are $c/U=-[(1+8/Fr)^{1/2}-1]/2$ (Thorpe & Kavčič 2008), tending to zero only as Fr tends to infinity. No stationary hydraulic jump without upstream wave propagation appears possible except when $\eta=0$; as for the η profile, $Fr_* \leqslant Fr_c$.

If a uniform shear is introduced above the stratified region, e.g. $u_1=U_0(h_1-z)/(H-h_1)$ in $h_1 \leqslant z \leqslant H$ and $u=-U_0$ in $z \geqslant H$, and the flow is as given in (1) and (2) with $i=1$ for $0 \leqslant z \leqslant h_1$, it can be shown that the boundary condition at $z=h_1$ for the stream function of the flow in $z \leqslant h_1$ remains unchanged in the long-wave limit. The eigenvalues c of the phase speed are therefore unchanged by the presence of the shear layer in the unstratified region $h_1 \leqslant z \leqslant H$. With the added shear layer, the 'extended η profile' replacing (27) is

$$F_1(x) = \begin{cases} 1, & \text{if } 0 \leqslant x \leqslant \eta\zeta, \\ 1+(1-\phi)(\eta\zeta - x)/[\zeta(1-\eta)], & \text{if } \eta\zeta \leqslant x \leqslant \zeta, \\ \phi(1-x)/(1-\zeta), & \text{if } \zeta \leqslant x \leqslant 1 \\ 0, & \text{if } x \leqslant 1 \end{cases} \tag{H 3}$$

and

$$f_1(x) = \begin{cases} 1, & \text{if } 0 \leqslant x \leqslant \eta\zeta, \\ (\zeta - x)/[\zeta(1-\eta)], & \text{if } \eta\zeta \leqslant x \leqslant \zeta, \\ 0, & \text{if } x > \zeta, \end{cases} \tag{H 4}$$

where $x=z/H$, $\zeta=h_1/H$ with $0<\zeta<1$ is a parameter that defines the relative thickness of the unstratified region of uniform shear, $V=U_1+U_0$ is the maximum flow speed (that in $0 \leqslant x \leqslant \eta\zeta$), and $\phi=U_0/V$ defines the magnitude of the flow in the uniform shear region. The Froude number of the extended η profile is

$$\boldsymbol{Fr} = V^2/g\Delta H = \zeta Fr/(1-\phi)^2, \tag{H 5}$$

where $Fr=U_1^2/g\Delta h_1$ is the Froude number of the η profile. For the extended η profile, (22) gives the smallest Froude number at which the conservation equations are satisfied:

$$\boldsymbol{Fr}_* = 2\zeta^2(1+\eta+\eta^2)/\{\zeta[1+2\eta+\phi(1-\eta)-\phi^2\eta]+\phi^2\}. \tag{H 6}$$

The values of $(-c/U_1)$ in figure 4 can be used to establish the value $\boldsymbol{Fr}=\boldsymbol{Fr}_c$ at which upstream wave propagation is just prevented. Since c is the same in the extended

flow as in the original η profile, the maximum upstream wave speed will be zero if $-c = U_0$. If, for example, $\eta = 0.5$, then from figure 4, $Fr = 1.6$ when $-c/U_1 = 0.1$. Putting $-c = U_0$, and using $\phi = U_0/V = U_0/(U_1 + U_0) = [(-c/U_1)/(1 + (-c/U_1)]$, we find $\phi = 0.1/1.1$, and (for this value of ϕ or U_0) $\boldsymbol{Fr}_c = \zeta 1.6(1.1)^2 = 1.936\zeta$, from (H 5). It follows, using (H 6), that $\boldsymbol{Fr}_c > \boldsymbol{Fr}_*$ for all ζ in the range 0–1.

No extended η profiles have been found for which $\boldsymbol{Fr}_c < \boldsymbol{Fr}_*$, when (22) would give the critical Froude number, the value beyond which a transition may occur with no upstream wave propagation.

REFERENCES

Baines, P. G. 1995 *Topographic Effects in Stratified Flows*. Cambridge University Press, p. 482.

Bell, T. H. 1974 Effects of shear on the properties of internal gravity waves. *Dtsch. Hydrograph Z.* **27**, 57–62.

Farmer, D. & Armi, L. 1999 Stratified flow over topography: the role of small-scale entrainment and mixing in flow establishment. *Proc. R. Soc. Lond.* A **455**, 3221–3258.

Ferron, B., Mercier, H., Speer, K., Gargett, A. & Polzin, K. 1998 Mixing in the Romanche fracture zone. *J. Phys. Oceanogr.* **28**, 1929–1945.

Hassid, S., Regev, A. & Poreh, M. 2007 Turbulent energy dissipation in density jumps. *J. Fluid Mech.* **572**, 1–12.

Holland, D. M., Rosales, R. R., Stefamica, D. & Tabak, E. G. 2002 Internal hydraulic jumps and mixing in two-layer flows. *J. Fluid Mech.* **470**, 63–83.

Hornung, H. G., Willert, C. & Turner, S. 1995 The flow field downstream of a hydraulic jump. *J. Fluid Mech.* **287**, 299–316.

Hoyt, J. W. & Sellin, R. H. J. 1989 Hydraulic jump as "Mixing Layer". *J. Hydraul. Engng* **115**, 1607–1614.

Klemp, J. B., Rotunno, R. R. & Skamarock, W. C. 1997 On the propagation of internal bores. *J. Fluid Mech.* **331**, 81–106.

Koop, C. G. & Browand, F. K. 1979 Instability and turbulence in a stratified fluid with shear. *J. Fluid Mech.* **93**, 135–159.

Lighthill, J. 1978 *Waves in Fluids*. Cambridge University Press, p. 504.

Mackinnon, J. A., Johnston, T. M. S. & Pinkel, R. 2008 Strong transport and mixing through the Southwest Indian Ridge. *Nature Geosci.* **1**, 755–758.

McEwan, A. D. & Baines, P. G. 1974 Shear fronts and an experimental stratified shear flow. *J. Fluid Mech.* 63, 257–272.

Osborn, T. R. 1980 Estimates of the local rate of vertical diffusion from dissipation measurements. *J. Phys. Oceanogr.* **10**, 83–89.

Peltier, W. R. & Caulfield, C. P. 2003 Mixing efficiency in stratified shear flows. *Annu. Rev. Fluid Mech.* **35**, 135–167.

Peregrine, D. H. & Svendsen, I. A. 1978 Spilling breakers, bores and hydraulic jumps. In *Proceedings of the 16th International Conference on Coastal Engineering*, ASCE, pp. 540–550.

Pham, H. T., Sarkar, S. & Brucker, K. A. 2009 Dynamics of a stratified shear layer above a region of uniform stratification. *J. Fluid Mech.* **630**, 191–223.

Polzin, K., Speer, K. G., Toole, J. M. & Schmitt, R. W. 1996 Intense mixing of Antarctic Bottom Water in the equatorial Atlantic Ocean. *Nature* **380**, 54–55.

St Laurent, L. C. & Thurnherr, A. M. 2007 Intense mixing of lower thermocline water on the crest of the mid-Atlantic Ridge. *Nature* **448**, 680–684, doi:10.1038/nature06043.

Saffman, P. G. & Yuen, H. C. 1982 Finite-amplitude interfacial waves in the presence of a current. *J. Fluid Mech.* **123**, 459–476.

Simpson, J. E. 1997 *Gravity Currents*, 2nd edn. Cambridge University Press, p. 244.

Stastna, M. & Lamb, K. G. 2008 Sediment resuspension mechanisms associated with internal waves in coastal waters. *J. Geophys. Res.* **113**, C10016, doi:10.1029/2007/JC004711.

Svendsen, I. B. A., Veeramony, J., Bakunin, J. & Kirby, J. T. 2000 The flow in weak turbulent hydraulic jumps. *J. Fluid Mech.* **418**, 25–57.

Swaters, G. E. 2009 Mixed bottom-friction-Kelvin–Helmholtz destabilization of source-driven abyssal overflows in the ocean. *J. Fluid Mech.* **626**, 33–66.

Thorpe, S. A. 1974 Near-resonant forcing in a shallow two-layer fluid : a model for the internal surge in Loch Ness. *J. Fluid Mech.* **63**, 509–527.

Thorpe, S. A. 2007 Dissipation in hydraulic transitions in flows through abyssal channels. *J. Mar. Res.* **65** (1), 147–168.

Thorpe, S. A. & Kavčič, I. 2008 The circular internal hydraulic jump. *J. Fluid Mech.* **610**, 99–129.

Thorpe, S. A. & Liu, Z. 2009 Marginal instability? *J. Phys. Oceanogr.* **39**, 2373–2381.

Thorpe, S. A. & Ozen, B. 2007 Are cascading flows stable? *J. Fluid Mech.* **589**, 411–432.

Thorpe, S. A. & Ozen, B. 2009 Corrigendum: are cascading flows stable? *J. Fluid Mech.* **631**, 441–442.

Thurnherr, A. M., St. Laurent, L. C., Speer, K. G., Toole, J. M. & Ledwell, J. R. 2005 Mixing associated with sills in a canyon on the mid-ocean flank. *J. Phys. Oceanogr.* **35**, 1370–1381.

Turner, J. S. 1973 *Buoyancy Effects in Fluids.* Cambridge University Press, p. 367.

Wilkinson, D. L. & Wood, I. R. 1971 A rapidly varied flow phenomenon in a two-layer flow. *J. Fluid Mech.* **47**, 241–256.

Yeh, H. 1991 Vorticity generation mechanisms in bores. *Proc. R. Soc. Lond.* A **432**, 215–231.